A synergy-based motor control framework for the fast feedback control of musculoskeletal systems

Reza Sharif Razavian*
Systems Design Engineering
University of Waterloo
Waterloo, Canada N2L 3G1
Email: rsharifr@uwaterloo.ca

Borna Ghannadi
Systems Design Engineering
University of Waterloo
Waterloo, Canada N2L 3G1
Email: bghannad@uwaterloo.ca

John McPhee
Professor, Fellow of ASME
Systems Design Engineering
University of Waterloo
Waterloo, Canada N2L 3G1
Email: mcphee@uwaterloo.ca

ABSTRACT

Summary: *This paper presents a computational framework for the fast feedback control of musculoskeletal systems using muscle synergies.* ***Method:*** *The proposed motor control framework has a hierarchical structure. A feedback controller at the higher level of hierarchy handles the trajectory planning and error compensation in the task space. This high-level task space controller only deals with the task-related kinematic variables, and thus is computationally efficient. The output of the task space controller is a force vector in the task space, which is fed to the low-level controller to be translated into muscle activity commands. Muscle synergies are employed to make this force-to-activation (F2A) mapping computationally efficient. The explicit relationship between the muscle synergies and task space forces allows for the fast estimation of muscle activations that result in the reference force. The synergy-enabled F2A mapping replaces a computationally-heavy non-linear optimization process by a vector decomposition problem that is solvable in real-time.* ***Results:*** *The estimation performance of the F2A mapping is evaluated by comparing the F2A-estimated muscle activities against the measured EMG data. The results show that the F2A algorithm can estimate the muscle activations using only the task-related kinematics/dynamics information with* $\sim 70\%$ *accuracy. An example predictive simulation is also presented, and the results show that this feedback motor control framework can control arbitrary movements of a 3D musculoskeletal arm model quickly and near-optimally. It is two orders-of-magnitude faster than the optimal controller, with only 12% increase in muscle activities compared to the optimal.* ***Conclusion:*** *The developed motor control model can be used for real-time near-optimal predictive control of musculoskeletal system dynamics.*

1 Introduction

The number of degrees-of-freedom (DoF) and the number of actuators (muscles) in the human body exceeds the minimum number required to perform various tasks. A task can be completed in a multitude of ways (the *degree of freedom problem*, [1]),

*Corresponding author

and a certain movement can be produced by an infinite number of muscle activation levels (the *muscle redundancy problem*). Various studies ranging from kinematic observations of limb movement [2, 3] to neuron activity decoding [4, 5, 6, 7] have suggested the importance of task-related variables in motor control.

How the muscles are activated to control the task variables is not fully understood. Optimization-based approaches have been proposed as a possible method to find muscle activations that produce a certain movement [8]. Although these optimization-based models can estimate the muscle activations reasonably well (e.g. [9, 10, 11]), their usefulness as a feedback motor control model is questionable. The optimization framework may work well in the context of well-practised motions, where the control can be viewed as feed-forward [12, 13, 14, 15]; however, it is not clear whether the nervous system is capable of continuously solving for the optimal muscle activations during the course of an action. The high computation cost of the optimization process renders it inapplicable for real-time control.

Non-optimal motion controllers for musculoskeletal systems have also been proposed. Examples include proportional-integral-derivative (PID) controllers [16, 17] and artificial neural networks (ANNs) [18, 19]. Combinations of these two types of controllers are proposed in [20] and [21]. These models, however, do not originate from biologically plausible motor control theory.

Among motor control theories, muscle synergy has gained some traction [22] as a biologically-plausible approach to simplify the muscle redundancy problem. According to this theory, the nervous system activates the muscles by combining a few activation sets (known as modules, synergies, or motor primitives). The literature is rich with studies that aim to extract these building blocks from measured muscle activations. A few examples include studies on healthy human movements [23, 24, 25, 26, 27, 28], motor learning and adaptation [29, 30], spinal cord injury [31, 32] and cerebral palsy patients [33], primates [34], frogs [35, 36, 37, 38, 39], and cats [40, 41, 42, 43].

In this large body of research, however, only a few studies have used muscle synergies to build motor control models to control the movements. In this area, the literature is limited to the study of simple tasks [15, 44, 45, 46, 47]. Among these, [15] and [46] have used a feed-forward scheme to drive a frog's hindlimb; [44] and [45] have employed sensory feedback but the intended tasks were simple, and they did not study multi-DoF movements. Finally, [47] have only implemented a torque-driven control scheme (with the motor synergies being joint torque profiles).

The literature in this field suggests that the control of movements occurs in the task space; muscle synergy theory is also proposed as a mechanism to simplify the control process. Despite the attempts made to create motion controllers for musculoskeletal systems, no comprehensive motor control model is available that includes all of the following features:

1. A feedback controller for the arbitrary movement of a general multi-DoF musculoskeletal system.
2. Task space control
3. Utilization of muscle synergies to simplify control
4. Real-time implementable

In this paper, we propose a general motor control framework that coherently combines all of the aforementioned features of the human motor control system. It includes a fast feedback controller in the task space for motion planning and error compensation. This framework is based on an explicit relationship between the muscle synergies and the task-related variables, which allows for fast estimation of the muscle activations from the task requirements. An important advantage of this mechanistic framework is its generalizability to arbitrary dimensions and tasks.

The organization of this paper is as follows. In the Method section, we introduce the proposed motor control framework, its subcomponents, and the underlying assumptions. Afterwards, the experimental trials designed to evaluate the predictive capabilities of the proposed framework are mentioned. We next demonstrate the capability of the motor control framework as a feedback motion controller in predictive musculoskeletal simulations using an example 3D upper extremity musculoskeletal model. In the end, the experimental and the simulation results are presented, which are followed by an in-depth discussion and conclusions.

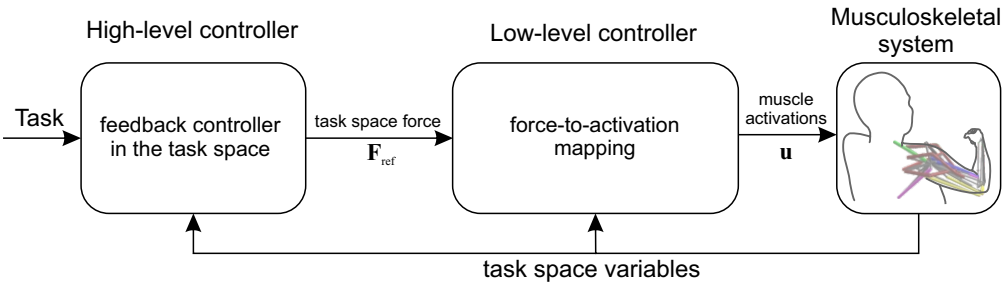

Fig. 1: The hierarchical structure of the proposed synergy-based motor control framework. The high-level controller is responsible for task space control, and outputs the task space force, $\mathbf{F}_{\text{ref}}$. The low-level F2A controller translates this force command to muscle activations, $\mathbf{u}$.

2 Method

Various observations suggest that the nervous system controls only the task-related kinematic variables [3]. Therefore, we speculate that the motor control system may store task-related representations of the body. To exemplify the distinction between the task-related and unrelated kinematic variables, consider a reaching task. Various shoulder/elbow angle combinations can result in the same hand position. In the reaching task, the hand position in space is the most important feedback to the motor control system, and individual joint angles are secondary to this task. Conversely, during an elbow flexion/extension task, the elbow angle is the kinematic variable that is being monitored and controlled. If the shoulder angle changes, the hand position will also change, but neither of these affect the elbow angle, and thus are irrelevant to the elbow flexion task. This view separates the control of the degrees of freedom that are related to the task from the ones whose variation does not affect the task, and eliminates the need for the nervous system to continuously solve an inverse kinematic problem.

Besides the task space representation, muscle synergies can further simplify the control process. An individual muscle, specifically a bi-articular muscle (muscles that span two joints, e.g. hamstring) may have a very complex function in the joint or task spaces, but the co-contraction of a number of muscles can potentially have a very clear task-related function. Therefore, the combination of the task-related representation of the body with the task/synergy relationship has a strong potential to simplify the motion control of musculoskeletal systems.

The details of the proposed computational motor control framework are presented in section 2.1. We have used an upper extremity reaching motion as the context to explain this framework. However, the framework is general and can be applied to any movement. In this context, the goal of the motor control framework is to handle the kinematic and dynamic redundancies of the arm in point-to-point reaching tasks. A constrained 2D reaching set-up (on a table surface) is used to experimentally evaluate the method (section 2.2). In a predictive simulation example (section 2.3), we have used a 4-DoF musculoskeletal arm model for 3D point-to-point reaching. Note that the experiments are used to evaluate the framework, while the simulations show its potential for predictive motion control.

2.1 Overview of the motor control framework

2.1.1 High-level controller

The hierarchical structure of the proposed motor control framework is shown in Fig. 1. In this framework, the task space is a vector space that contains all the task-related kinematic variables (e.g. the (x,y,z) position of the hand in a reaching task). The high-level controller is a feedback controller in the task space, which only deals with the task variables, and disregards the complexities of the musculoskeletal system. Its role is to compare the current task variables with the target, and define the reference task space forces ($[\mathbf{F}_{\text{ref}}]_{p\times 1}$ where p is the task space dimension) required to achieve the goal. For the sake of simplicity, we have chosen a PID controller that handles error compensation. More complex task space controllers are beyond the scope of the present study, but the implications are discussed in section 4.

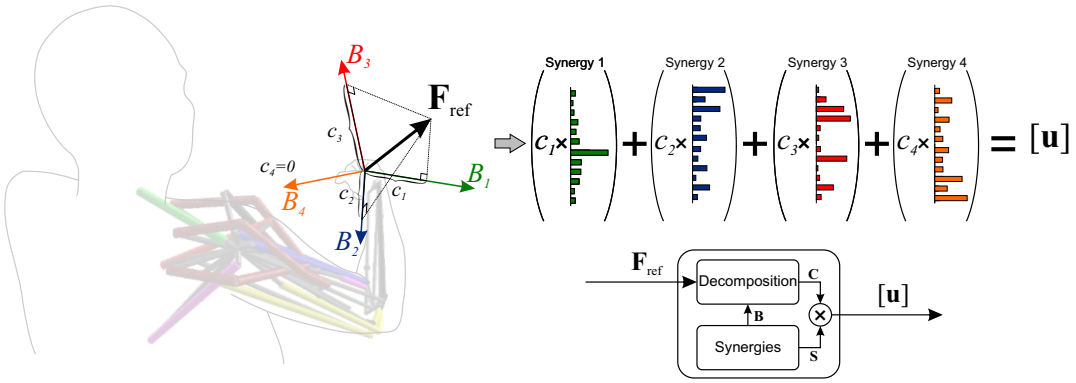

Fig. 2: The schematic of the force-to-activation (F2A) mapping. An arbitrary force vector (black arrow, $\mathbf{F}_{\text{ref}}$) can be decomposed onto the basis set (coloured vectors, B_i) to find the corresponding coefficients. The same coefficients can then be used to combine the synergies to calculate the muscle activities, $\mathbf{u}$, that result in the reference force, $\mathbf{F}_{\text{ref}}$. In this illustration, the task space is 3D ($p = 3$), and only four synergies ($k = 4$) are shown to demonstration the concept.

Note that the task space controller only defines the forces in the task space, which leaves the motion of redundant DoF uncontrolled. Our approach to separate the control of task and redundant DoFs is briefly explained in section 2.1.3 and fully provided in [48, 49, §3.2.2].

2.1.2 Low-level controller

Human motions are produced by muscle contractions. Thus, the reference force specified by the task space controller needs to be translated to muscle activations (see Fig. 1). Muscle synergies can been used to simplify the calculations in this force-to-activation (F2A) mapping. Essentially, we view muscle synergies as the pre-calculated sets of solutions for the muscle force sharing problem (perhaps obtained through evolution or practice). The details on how one might obtain these synergies will be provided later in this paper, but for now, we assume the synergies are known. The way our F2A mapping works is depicted in Fig. 2 and described below.

We assume that the motor control system contains k synergies for a given task, represented in our model by the matrix $\mathbf{S}_{m\times k}$, where each column of $\mathbf{S}$ contains the relative activation of the m muscles in a single synergy (i.e. $s_{i,j}$ is the activation level of the i^{th} muscle in the j^{th} synergy). It is also assumed that the effect of each synergy in the p-dimensional task space is known (e.g. we know that activation of synergy 1 in Fig. 2 results in a task space force $[B_1]_{p\times 1}$). The collection of these synergy-produced force vectors can be viewed as a *basis set*, $\mathbf{B}_{p\times k} = [B_1, B_2, \ldots, B_k]$, for the task space. In other words, any arbitrary force vector in the task space can be created by a linear combination of these basis vectors. Thus, the nervous system can *decompose* the reference force vector, $\mathbf{F}_{\text{ref}}$, onto this basis set, to calculate the coefficients (i.e. intensity) of each basis vector. This process is analogous to solving for the coefficients vector $\mathbf{C}_{k\times 1}$ in the following equation:

$$[\mathbf{F}_{\text{ref}}]_{p\times 1} = \mathbf{B}_{p\times k}\mathbf{C}_{k\times 1} \tag{1}$$

which can be solved using a non-negative least-squares algorithm.

The basis vectors combined with the coefficients c_i produce the reference force. Likewise, the synergies (that produce the basis vectors) combined with the same coefficients result in the muscle activations that produce the reference force; i.e.,

$$\mathbf{u}_{m\times 1} = \mathbf{S}_{m\times k}\mathbf{C}_{k\times 1} \tag{2}$$

is the solution of the muscle force sharing problem. The proposed F2A mapping has an important implication: *it replaces the costly and time-consuming non-linear optimization process with a linear vector decomposition problem to solve the muscle force sharing problem*. As a result, it is possible to implement this method for real-time motion control. Although this method may not always give optimal results, our dynamics simulation results (section 2.3) show that they are near-optimal. The block diagram of the F2A process is also shown in Fig. 2.

2.1.3 Control of redundant and non-redundant degrees of freedom

The proposed framework can be applied to a system without kinematic redundancy, where the motion in the task space fully defines the kinematics of the system. However, in kinematically redundant systems, there are extra degrees of freedom that can vary without affecting the task space motion. To control the task-related kinematics and leave the redundant ones uncontrolled, it is possible to define synergies that produce forces only in the task space (an example method for achieving this requirement is presented later in section 2.3.2). In this way, the employed synergies do not induce any extra motion in the redundant space, and allow it to move as a natural result of interaction with the environment.

If it is necessary to control these redundant DoFs (e.g. to reach to an object in a certain angle), we can employ an extra set of synergies that produce forces only in the redundant space. These two orthogonal sets of synergies (the task space ones and the redundant space one) enable the framework to separately control the movement in the two spaces (see [48, 49, §3.2.2] for more details).

2.1.4 The underlying assumptions

Positive-decomposition. Muscles are pull-only actuators. Thus, only a positive muscle activation level is meaningful. The same property is also assumed for a synergy; i.e. a synergy cannot have a negative coefficient. Therefore, the vector decomposition mentioned above has to be a *positive decomposition* ($c_i > 0$). This assumption itself implies that at least four synergies are needed to positively decompose a force vector in the 3D task space (in general, $p+1$ synergies for a p-dimensional task-space).

Task-specific synergies. We have assumed a tight relation between the synergies and the task (as was previously suggested in [45]). The term *task-specific synergies* means that, for example, the synergies employed during a 3D reaching task (controlling the hand position) are different from the ones during elbow flexion (controlling elbow angle). The uncontrolled manifold theory [3] can help distinguish between different tasks by identifying the actively controlled variables.

Principle of superposition. Our method (and muscle synergy theory in general) relies on the principle of superposition. Under certain assumptions (body is stationary, and the elasticity of the muscles are neglected), the relationship between the muscle activities and the resulting task space force is linear, and superposition can be applied—the effect of co-activation of multiple synergies (i.e. the total task space force) is the same as the summation of the effects of individual synergies (i.e. the basis vectors). When the velocities are not negligible, it is possible to account for the non-linear dynamics using a dynamic model of the arm [49, 50], which however, is not included in this paper.

2.2 Evaluation of the framework (F2A mapping) with human experiments

This section describes the experimental procedure designed to evaluate the performance of the computational motor control framework. Specifically, we evaluated how well the F2A mapping could recreate muscle activities only using the task space measurements. Therefore, it was assumed that the movements were governed by a high-level controller; the nature of this controller was not the focus of this experiment. Instead, the goal was to employ the F2A methodology to estimate the muscle activities from the measured task space kinematics/dynamics, and compare the results with the measured electromyography (EMG) data.

For this purpose, the set-up shown in Fig. 3a was used. This set-up included a two-DoF haptic robot (Quanser Inc.) that allowed motion in the horizontal (table top) plane. The subject was asked to hold and move the robot end-effector. Therefore, the task space was the 2D (x,y) position of the hand/end-effector. The end-effector was equipped with a six-axis force sensor (Nano25, ATI Industrial Automation, Inc.) to measure the task space forces. The end-effector position was also measured

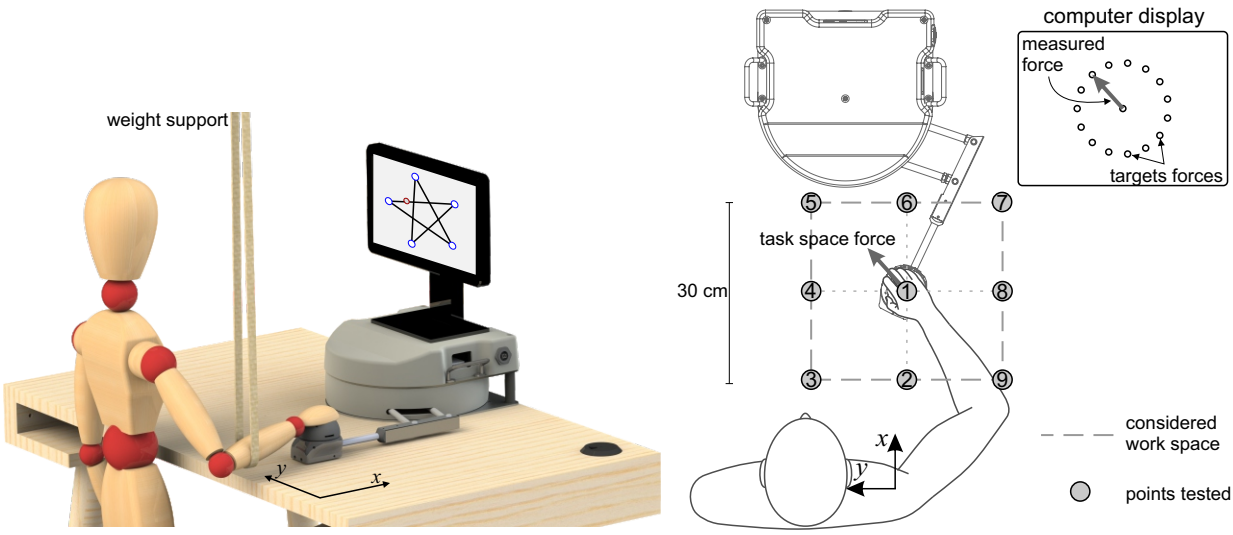

(a) (b)

Fig. 3: (a) The experimental set-up includes a 2DoF haptic robot to measure force/position in the 2D task space. The arm is lifted above the table surface to support its weight and minimize friction. (b) The set-up configuration in phase one of the experiment. The robot is locked in any of the 9 points in the task space, and the subject has to match the target forces by pushing against the robot.

by the robot. The subject's arm was suspended to remove the effects of gravity and arm/table friction (arm does not move off-plane). The robot's control loop and the force sensor had a 500 Hz sampling rate.

Surface EMG data from seven muscles (anterior/middle/posterior deltoid, biceps brachii, brachioradialis, and long/lateral heads of triceps brachii) were recorded at 1926 Hz (Trigno Wireless EMG, Delsys Inc.). The EMG data was processed with the common procedure: raw EMG $\rightarrow$ zero-mean $\rightarrow$ band-pass filter with 6th-order Butterworth and 5-800 Hz cut-off frequencies $\rightarrow$ full-wave rectify $\rightarrow$ low-pass filter with 6th-order Butterworth and 2 Hz cut-off frequency. The bandpass filter cut-off frequencies were chosen so as to remove the biases in the signals while retaining as much information as possible using Fast Fourier Transform (FFT). The low-pass filter (linear envelop) cut-off frequency was fixed at 2 Hz to obtain smooth signals, considering that the tested actions were free of rapid changes in muscle activities. The EMGs for each muscle were normalized with respect to the maximum voluntary contraction (%MVC) [51].

The experiment was conducted in two phases. In phase one (the *off-line* phase), the synergies were obtained and stored. In phase two (the *on-line* estimation phase), these synergies were used in the F2A algorithm to reconstruct the muscle activities during arbitrary motions.

Seven young and healthy subjects (five male, two female, average age 26.7 ± 2.9, all right-handed) participated in the experiment. All subjects reported no musculoskeletal disorder in the past 2 years. This study was carried out in accordance with the recommendations of the Office of Research Ethics at the University of Waterloo with written informed consent from all subjects.

2.2.1 Phase one: off-line calculation of the synergies

The robot end-effector was locked in 9 different positions in the task space (a 3×3 grid, with the order shown in Fig. 3b), and in each position, the subject isometrically applied forces to the end-effector. A computer display visualized the measured force vector as a point, which the subject had to match with multiple targets. The target forces were 12 N along 15 equally-spaced directions (in a circular pattern, Fig. 3b) in the horizontal plane. The subject had to hold the force for at least 2 s within 10% accuracy range to successfully match a target. The subject was instructed to rest their arm on the armrest throughout the experiment.

In every tested posture, the EMG data from seven muscles and for each force direction was averaged in the 2-s window

prior to the successful target matching. The collection of these data for all 15 targets formed the data matrix $\mathbf{A}_{7\times15}$.

According to muscle synergy theory, the data matrix $\mathbf{A}$ is produced by a linear combination of a small number of synergies. Non-negative matrix factorization (NNMF, originally proposed in [52]) has widely been used to extract the synergies from such a data matrix, and is used in this work to define the synergies. It must be noted that any alternative method to define the synergies is applicable as well (for a review of alternative factorization algorithms see [53]). The NNMF finds the synergy matrix $\mathbf{S}$ and the coefficient matrix $\mathbf{C}$ with non-negative elements, such that their product best approximates the matrix $\mathbf{A}$.

$$\mathbf{A}_{7\times15} \simeq \mathbf{S}_{7\times k}\mathbf{C}_{k\times15} \tag{3}$$

or

$$\text{minimize: } e = \text{norm}(\mathbf{A}_{7\times15} - \mathbf{S}_{7\times k}\mathbf{C}_{k\times15}) \tag{4}$$

with k being the number of muscle synergies.

In this formulation, each column of the synergy matrix represents a single synergy; $s_{i,j}$ contains the activity level of the i^{th} muscle in the j^{th} synergy. A column in the coefficient matrix contains the coefficients of the synergies for a specific target ($c_{i,j}$ is the coefficient of the i^{th} synergy for the j^{th} target).

The basis set $\mathbf{B}$ corresponding to a synergy matrix was also obtained by solving the equation:

$$\mathbf{F}_{2\times15} = \mathbf{B}_{2\times k}\mathbf{C}_{k\times15} \tag{5}$$

using a least-squares method, where the matrix $\mathbf{F}_{2\times15}$ contained the measured 2D force vectors in the 15 directions.

Applying this process to the data matrix $\mathbf{A}$ and force matrix $\mathbf{F}$ in another posture resulted in new synergy/basis matrices. Therefore, this procedure gave us *posture-dependent* synergies and bases defined as $\mathbf{S} = \mathbf{S}(x,y)$ and $\mathbf{B} = \mathbf{B}(x,y)$, with (x,y) being the hand position in the task space.

2.2.2 Phase two: motion trials and on-line estimation of muscle activation

Next, the subject performed multiple point-to-point reaching motions in the 2D task space. The movement resembled 10 repetitions of drawing a five-pointed star, where each repetition included five point-to-point segments of length 28 cm. As a visual feedback, the subject could see the current location of the hand on the screen and the next target. No instruction regarding the speed of motion was given to the subject, but they were asked to avoid sudden movements and perform smooth movements. To increase the muscular activities, the robot resisted the motion similar to a linear damper with damping coefficient of 250 N.s/cm The task space forces and positions were recorded in synchrony with EMG during the movements. At each point during the motion, the posture-specific synergy and basis matrices were estimated by interpolating the previously obtained matrices (using cubic spline interpolation). Then, the measured force vector was decomposed onto the basis set (similar to (1)) to calculate the corresponding coefficients, which were multiplied by the synergy matrix to reconstruct the muscle activities. The only data available to this mapping were: the real-time measurement of the task space force (F_x, F_y) and position (x,y), as well as the synergy and basis matrices ($\mathbf{S}$ and $\mathbf{B}$) previously obtained off-line.

To quantify the estimation performance, the *variance accounted for* (VAF) [54, 55] is calculated:

$$VAF = 1 - \frac{\sum(u-\hat{u})^2}{\sum u^2} \tag{6}$$

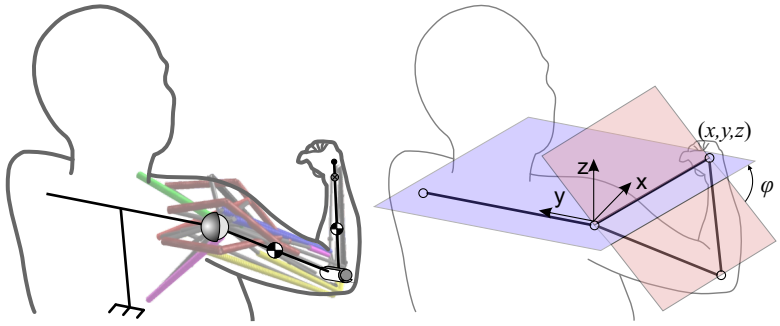

(a) (b)

Fig. 4: **(a)** The schematic of the 3D 4-DoF arm model. **(b)** The 3D task space, containing (x,y,z) position of the hand, and the redundant space containing the kinematic variable ϕ. Here, the rotation specified by the angle ϕ is irrelevant to the reaching task.

where the summation is across the entire duration of the movements. $\hat{u}$ denotes the estimated muscle activities using the presented synergy approach, which is compared against the gold standard, u (in this case the measured EMGs). The experimental results are presented in section 3.

2.3 The motor control framework for predictive musculoskeletal simulations

The framework's computational efficiency makes it an ideal platform to produce fast dynamic simulations of musculoskeletal systems without the need to define any motion as the input. In this section we show a simulation example to demonstrate the potential of the proposed motor control model as a predictive feedback motion controller for musculoskeletal simulation. In contrast to the 2D experimental setup, we have used a 4-DoF musculoskeletal arm model; the goal is to reach arbitrary targets in 3D space with the hand. Because of the differences in the experimental and simulation set-ups, the two sets of results are not compatible and are not compared in the Results section.

2.3.1 The musculoskeletal model

A 3D musculoskeletal arm model [56] is used to demonstrate our motor control framework (see Fig. 4a). In this model the torso is fixed, to which the upper arm is connected via a spherical joint (3-DoF). The elbow is a 1-DoF revolute joint connecting the forearm/hand to the upper arm (wrist is fixed). As a result, this 3D arm model has four DoFs.

This arm model is actuated by 15 muscles (listed in [56]), which are modelled using the Hill-type formulation [57]. For simplicity, only the contractile element of the muscle model is implemented. The input to the model, u, is the set of muscle activations, which result in muscle forces that generate the motion (forward dynamics simulation).

In this example, the intended task is to reach to an arbitrary target in 3D space with the hand. Therefore, the *task space* is a 3D vector space containing (x,y,z) variables. Since the arm model has four DoFs, there remains one extra DoF that is unrelated to the task; thus, the *redundant space* is a 1D vector space containing the extra variable (ϕ in Fig. 4b).

To implement the motor control framework in a musculoskeletal simulation context, we first need to define the synergies appropriately.

2.3.2 How to calculate synergies

The presented motor control framework can be used with any sets of muscle synergies, as long as they are rich enough to *positively* span[1] the intended task space. Any method that calculates such synergies and bases may be used to work with this framework. Because the number of muscles and task spaces are different in the 3D reaching simulating and the 2D experiments, the experimentally obtained synergies cannot be used here. Below we explain an *off-line* method to calculate and store the synergies in a simulation setting, which can then be used in feedback control of movements in forward dynamics

[1] by positive span we mean that any arbitrary vector can be positively decomposed onto the basis set

simulation of musculoskeletal systems. It must be noted that task space *acceleration vectors* were used instead of force vectors due to the ease of implementation (therefore, we have *acceleration-to-activation*, or A2A mapping in the simulations instead of F2A).

A large number of optimization problems are solved to mimic the human evolution/practice process to obtain and store the synergies prior to the feedback control process. At a given posture (defined by (x, y, z, ϕ), see Fig. 5), the best combination of muscle activities that produce a certain task space acceleration is found through an optimization process. The optimization algorithm (in our simulations we used sequential quadratic programming) finds the vector of m muscle activations, $\mathbf{u}_{m\times 1}$, that minimize the following objective function:

$$\mathbf{u}_{m\times 1} = \arg\min \left\{ J = \omega_1 \frac{1}{|\mathbf{a}_{des}|^2} |\mathbf{a}_{des} - \mathbf{a}|^2 + \omega_2 \mathbf{u}^T \mathbf{u} \right\} \tag{7}$$

Here, J is the objective function that is minimized. $\mathbf{a}_{des}$ and $\mathbf{a}$ are the desired and actual hand acceleration vectors, respectively. ω_1 and ω_2 are the weighting factors that balance the importance of the tracking error and the muscular effort terms. The optimization is subjected to the constraints:

$$0 \leq u_i \leq 1 \quad , i \in \{1, .., m\} \tag{8}$$

and

$$\ddot{\phi} = 0 \tag{9}$$

The constraint (9) forces the solution to produce zero acceleration in the redundant space. This assumption simplifies the computations when the intent is to control the task space movements only.

The same optimization process is repeated for $n = 30$ different acceleration vectors in various directions (see Fig. 5). The solutions of these optimization problems are then gathered in a matrix $\mathbf{A}$ as:

$$\mathbf{A}_{m\times n} = [\mathbf{u}_1, \mathbf{u}_2, \ldots, \mathbf{u}_n] \tag{10}$$

This data matrix can then be broken into the synergy and coefficient matrices using NNMF:

$$\mathbf{A}_{m\times n} \simeq \mathbf{S}_{m\times k} \mathbf{C}_{k\times n} \tag{11}$$

where each column of the synergy matrix represents a single synergy; $s_{i,j}$ contains the share of the i^{th} muscle in the j^{th} synergy.

Applying the NNMF to the solution matrix $\mathbf{A}$ gives a set of synergies at the current posture. If the entire process is repeated for various hand positions/orientations in the working space, a set of posture-dependent synergies can be defined (i.e. $\mathbf{S} = \mathbf{S}(x, y, z, \phi)$). In the simulations, we solved for the synergies in a 4-dimensional grid of $5 \times 5 \times 5 \times 6$ points corresponding

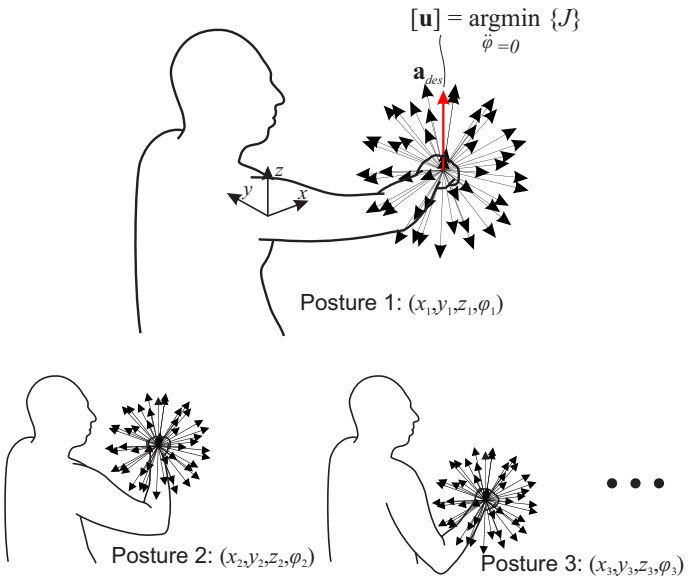

Fig. 5: A large number of optimization problems are solved off-line to obtain the synergies that are used in the simulations. In a given posture, an optimization is solved to find the optimal muscle activations that produce each of the desired task space accelerations ($\mathbf{a}_{des}$). The same process is repeated for a variety of postures.

to (x, y, z, ϕ) dimensions.

These posture-dependent synergies and the corresponding task space basis vectors are assumed to be stored in the nervous system. During motion control, they are recalled and interpolated (cubic spline method) in the A2A mapping to estimate the synergy coefficients, and consequently muscle activations. The constraint $\ddot{\phi} = 0$ in (9) ensures that the set of activations obtained from the A2A mapping does not induce extra acceleration in the redundant space (i.e. to leave it uncontrolled). This assumption also simplifies the computations when the redundant DoF needs to be controlled as well [48, 49, §3.2.2].

2.3.3 Simulation study design

In the presented example, the motor control framework is used to control the motion of the 3D and 4-DoF musculoskeletal arm model. The target motion in the simulation is a 20 cm hand elevation in the z direction (against gravity). Two feedback control methods are used to produce this motion: the proposed motor control framework, and a non-linear model predictive controller (NMPC) [58]. The NMPC is an optimal (but computationally expensive) feedback controller that is considered as the baseline, against which the synergy-based controller is compared. The NMPC is implemented with a 3-step prediction horizon. In each time step, a *sequential quadratic programming* algorithm calculates the optimal muscle activations that minimize the following cost function:

$$J_{nmpc} = w_1 \sum_{i=1}^{m} \left(\int u_i^2 dt \right) + w_2 \int (e_p)^2 dt + w_3 \int (e_v)^2 dt + w_4 \int (e_\phi)^2 dt \tag{12}$$

In this cost function, which is calculated for the upcoming prediction window, the first term is responsible for keeping the muscle activations low, while the second and third terms ensure tracking of the reference trajectory (e_p and e_v are the position and velocity error). The last term ($\int (e_\phi)^2 dt$) handles tracking in the redundant space. The weighting factors, w_i's, indicate the relative importance of the cost function terms. Numerical values of the PID (the high-level controller in the framework) and NMPC parameters are given in Table 1.

Table 1: The musculoskeletal simulation parameters

Parameter	value
PID coefficients	$K_p = 3000\ (s^{-2})$
	$K_d = 100\ (s^{-1})$
	$K_i = 1500\ (s^{-3})$
NMPC weightings	$w_1 = 1(s^{-1})$
	$w_2 = 1 \times 10^5\ (s^{-1}m^{-2})$
	$w_3 = 1 \times 10^4\ (sm^{-2})$
	$w_4 = 1 \times 10^5\ (s^{-1})$

The simulations are performed on a desktop computer (CPU Intel Core i7-4790, RAM 16GB, 64-bit Windows 7) running MATLAB/Simulink 2014b. The musculoskeletal model was developed in MapleSim 7, which was exported as C-code to run in MATLAB.

3 Results

In this section we present the results corresponding to the experimental trials and the simulations. The 2D experimental results are meant to evaluate the motor control framework performance in estimating muscle activations from the task space measurements, while the 3D simulation results show its application to predictive musculoskeletal simulations. The simulation and experimental results illustrate different aspects of the proposed method, and are not meant to be compared.

3.1 Experimental results

The detailed experimental results for subject #2 are shown here (Fig. 6). Applying the NNMF algorithm to the posture-dependent EMG data-sets results in the posture-dependent synergies that are shown in Fig. 6a (the results with three synergies, $k = 3$, are shown here). Each surface in the visualization of the synergies shows the variation of a muscle's activation level in a synergy across various positions in the 2D task space. Fig. 6b shows the corresponding synergy-produced basis vectors in nine representative positions in the 2D task space. The point-to-point motion trials in the 2D task space (average velocity 3.8 ± 0.6 cm/s for this subject) and the associated task space forces are shown in Fig. 6c. A *segment* is the movement from one target to the next (5 targets in total), and the motion in each segment was repeated 10 times. Finally, the measured EMGs during the movements are shown in Fig. 6d, super-imposed by the activations estimated from the presented method. The calculated VAF (6) for each muscle and in each movement segment is given above each individual plot. The numbers on the right and bottom of the panels show the weighted average VAF, calculated as:

$$VAF_{ave} = \frac{\sum(\overline{emg}.VAF)}{\sum \overline{emg}} \tag{13}$$

where $\overline{emg}$ is the average value of the recorded EMG for a muscle during a segment of the motion. The summations in (13) are taken across various segments for a given muscle (resulting in average numbers shown below the panels for an individual muscle), or various muscles for a given segment (resulting in average numbers to the right of the panels for each segment), or all segments and muscles (resulting in the total VAF on the bottom right corner).

The motor control framework presented here is a general method; however, the results (specifically the synergies) are subject-specific, and inter-subject comparison is difficult. Therefore, only the details of one subject's results are shown here

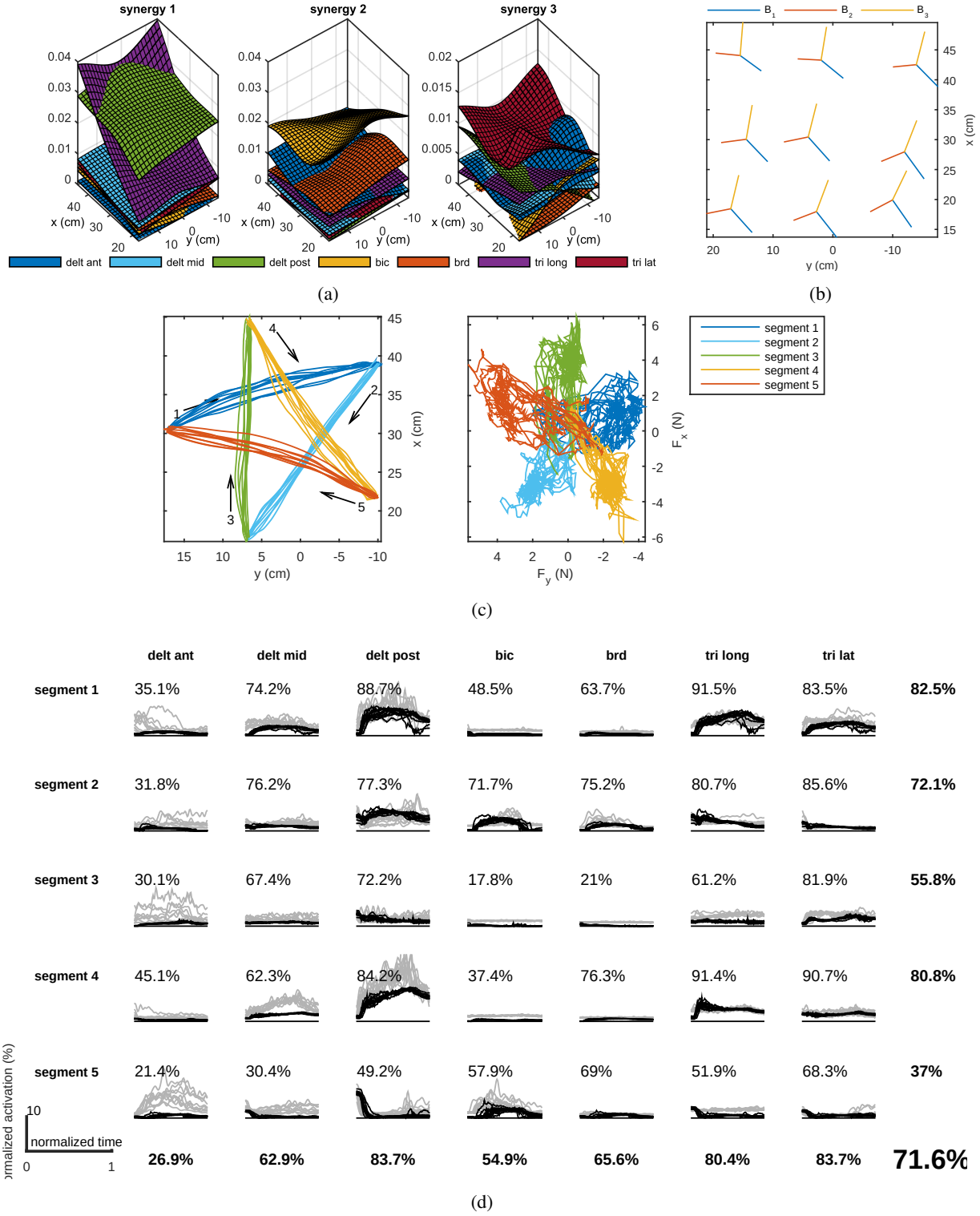

Fig. 6: **The 2D experimental results.** The data belongs to subject #2. **(a)** The synergies obtained by applying the NNMF to the experimentally measured EMG data. Each plot shows how the activity level of the muscles (color coded) in a synergy change across posture. **(b)** The basis vectors associated with the posture-dependent synergies. **(c)** The motion and force in the task space during the motion trials. The motion is divided into 5 segments (color coded). **(d)** The measured EMG and the reconstructed activations for the seven muscles and for each motion segment. The grey and black lines, respectively, show the measured EMG data, and the reconstructed muscle activations. Each line represents a single trial. The numbers in each plot give the calculated VAF. The bold numbers on the right and the bottom are the average for the row or column of data, respectively. The single large number on the bottom right is the average of all VAF measures.

Table 2: Calculated total VAF values in the experimental evaluation of the framework

Subject #	VAF (%)	Subject #	VAF (%)
1	87.1 ± 0.6	5	76.8 ± 0.2
2	71.6 ± 0.3	6	70.6 ± 0.2
3	73.5 ± 0.7	7	60.9 ± 0.1
4	47.3 ± 0.5		
Average of all subjects: 69.7 ± 12.6			

Table 3: The timing details of the motor control framework and the optimal controller to simulate 1.5 s motion

Simulation type	Optimal	Synergy
Musculoskeletal model run time	47 ms	47 ms
Controller run time	55567 ms	Low-level (A2A): 702 ms High-level (PID): 31 ms Total: 733 ms

(the results for other subjects are available in the supplemental material). To make inter-subject comparison, the calculated average VAF is used. Table 2 gives the average VAF for all seven subjects. Because each run of NNMF may result in a different synergy set, 10 runs are performed and the mean±standard deviation of the results are reported.

3.2 Simulation results

The application of the proposed motor control framework to predictive musculoskeletal simulations is presented here. The simulation set-up is as described in section 2.3.3, and the results are shown in Fig. 7. Fig. 7a visualizes the five extracted synergies and how the activation level of the muscles in the synergies change across various postures. Fig. 7b shows the synergy-produced basis vectors in the 3D task space in a representative posture $(x, y, z, \phi) = (15cm, -20cm, -20cm, 0^\circ)$.

Two control methods are compared in Figs. 7c and 7d: the synergy-based motor control model and the optimal NMPC, denoted by "synergy" and "optimal", respectively. The arm motion resulting from the two controllers is shown in Fig. 7c, along with the muscle activations presented in Fig. 7d. Note that the synergy-based controller leaves the redundant DoF (ϕ) uncontrolled, and the arm falls due to gravity. To obtain comparable results with the optimal controller, it was required to follow the same ϕ trajectory.

The muscle activations in Fig. 7d show that the motor control framework is able to predict activity of the highly-activated muscles (e.g. deltoid) as well as the less active ones (e.g. supraspinatus). However, there is occasional overestimation (e.g. triceps and pectoralis major). The results show that the physiological effort ($= \int \mathbf{u}^T \mathbf{u} dt$) from the synergy controller is only 11.6% more than that of the optimal controller, while the computation time reduced by two orders of magnitude(the timing details are given in Table 3).

3.3 Number of synergies

The effect of the number of synergies on the framework performance (VAF in (6)) as well as the NNMF error (e in (4)) is shown in Fig. 8. The gold standard in the calculation of VAF for the experimental and simulation results are, respectively, the EMGs and optimal muscle activations. The results in Fig. 8a represent subject #2's data.

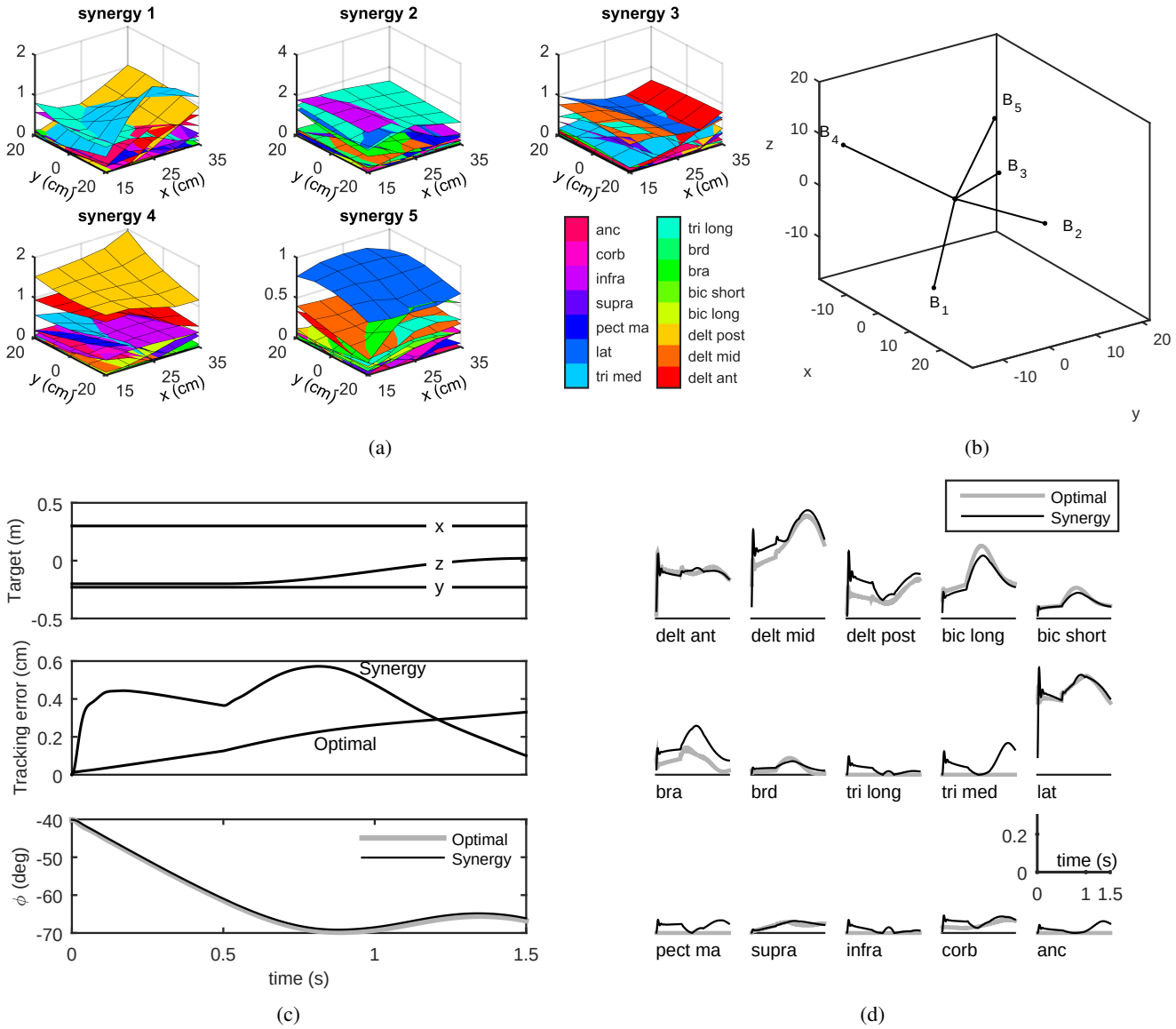

Fig. 7: **The 3D simulation results.** **(a)** The synergies visualized in the task space. Each plot shows the activity level of the 15 muscles (color coded) in a synergy, as the hand moves in the task space. The x and y axes indicate the position of the hand (cm), and the vertical axis shows the muscle share in a synergy. These plots belong to the posture where the hand's vertical position is 20 cm below the shoulder ($z = -0.2\ m$), and $\phi = 0°$. More detailed synergy plots are available in the supplementary materials. **(b)** The basis vectors in the task space. The units are m/s^2. These basis vectors belong to the posture $(x, y, z, \phi) = (15cm, -20cm, -20cm, 0°)$. **(c)** The trajectory for the hand position (moving 20 cm upwards), the tracking error, and the motion in the redundant space. Two control methods are compared: an optimal controller, and the synergy-based motor control model. **(d)** The muscle activations resulting from the two control methods.

4 Discussion

The presented motor control framework is a computational tool developed to facilitate predictive forward dynamics musculoskeletal simulations. Unlike other synergy-based forward dynamics simulations (e.g. [9, 12, 15, 59]), in which a feed-forward control scheme was used, the presented framework employs feedback information to calculate and adjust the muscle activation levels. A key advantage of this motor control framework is that it can handle feedback control of musculoskeletal systems in real-time and near optimally. This motor control model was found to be capable of estimating muscle activities that are close to the measured EMG data (VAF $\approx 70\%$), and optimal activations (VAF $\approx 90\%$).

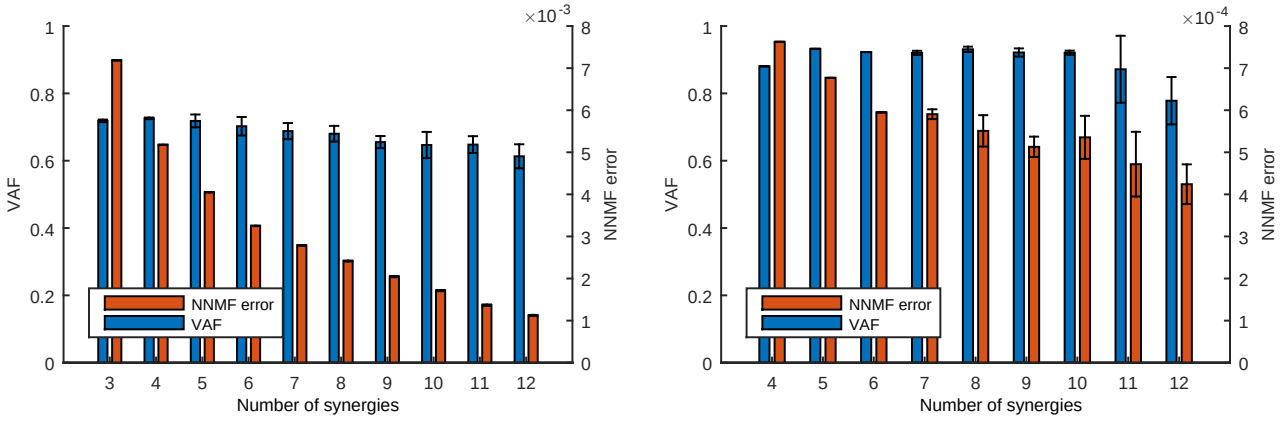

(a) Experiment (b) Simulation

Fig. 8: The effect of number of synergies on the performance of the motor control framework. **(a)** The experimental results belonging to subject #2. **(b)** The simulation results. Because the NNMF is sensitive to the initial guesses, multiple runs of NNMF are performed. The plots show the mean and standard deviation of the results. When a small number of synergies are used, the variability is small.

4.1 Task space controller

The presence of task-related kinematics in the motor control system is widely reported in the literature [4, 5, 6, 7, 60, 61, 62, 63]. Our motor control framework is inspired by these observations and creates a simple feedback control loop solely based on the task-related variables. In the example simulation shown (3D reaching), the obvious choice of the task-related kinematics was the hand position in space. However, in more complex movements (e.g. sit-to-stand), the choice of task space is not so obvious. The uncontrolled manifold theory [3] provides a useful tool to rank the kinematic variables and identify the actively controlled ones.

It is also worth noting that subtle changes in the goals of the task may alter the underlying control mechanisms. For instance, during a normal reaching task, the goal is to move from one point to another; however if a joint is causing pain, another important goal is to restrict its motion. In our framework, this would be a new and more complex task space, which would engage a different set of high/low level controllers.

Similar to the idea proposed in [44], the task space controller chosen in our simulations was an error-driven PID controller. Despite showing acceptable results in the simulations, it might not capture important properties of the human motor control system, such as prediction/expectation, adaptability, and robustness. More complex feedback controller types, such as optimal (e.g. Model Predictive Controller [58], or Linear Quadratic Gaussian [64]), or robust/adaptive controllers, may be used to model the task space controller.

4.2 Force-to-activation mapping

The force-to-activation mapping presented here is a key component of the computational motor control framework. This methodology assumes no restriction on the number of DoFs, the task space dimensions, and whether the system is kinematically redundant or not. Our results showed its application to 2D (experimental) and 3D (simulation) task spaces. Since the two task spaces in the experiment and simulations were different, two separate sets of synergies were used (the same set could not be used). Furthermore, the presented simulation results should be viewed as an example of motion control for a complex musculoskeletal system, and are not meant to be compared against the experimental results.

The performance of the F2A mapping depends on the number of synergies and how well the task space is spanned by the basis vectors. It was shown in [55] that a low decomposition error (e in equation 4) did not translate well to the task space performance. The NNMF does not take into account the task space (i.e. the basis vectors in Figures 7b and 6b), and may result in a non-optimal distribution of basis vectors when a high number of synergies are used. Therefore, counter-intuitively, more synergies do not improve the overall performance, despite the decrease in NNMF error (Fig. 8).

Posture dependency is another important assumption in our motor control framework. The generalizability of static synergies across various postures has been discussed before (e.g. in [42, 40]). However, the added flexibility of the posture-dependent synergies (as opposed to the fixed ones) allows for a smaller number of synergies to be used. The posture-dependence assumption is in agreement with the observations in [65] that the habitual muscle activation patterns to produce the same amount of wrist force change with its pronation angles.

The posture dependence feature requires the synergies to be calculated at a number of postures in the work space. In general, the quality of control is expected to increase by solving for the synergies at a larger number if postures. However, increasing the number of data points for synergy interpolation is costly. The number of postures to consider depends on how large the intended workspace is, and how fine the mesh should be to give good interpolated results. The simulated synergies in Fig. 7a were obtained with a 10 cm mesh spacing in the task space. A finer mesh did not significantly improve the results.

The VAF values reported in Fig. 6d for individual muscles and segments show excellent prediction for some muscles (e.g. $> 90\%$ for triceps muscles during segments 1 and 4 where they are the major movers), and poor prediction for some others (e.g. biceps and brachioradialis in segment 3 where they are inactive.) The inconsistency between the measurement and prediction is mostly attributed to the unreliability of measured EMG (e.g. at low activity levels; also note the inconsistency of the EMG data in various repetitions for anterior deltoid in Fig. 6d).

There are limitations in the F2A mapping, including its inability to account for antagonist muscles co-contraction (e.g. for limb stabilization as proposed in [66]), secondary movements (e.g. the movements in the redundant degrees of freedom, [48, 49, §3.2.2]), and velocity dependence of muscle force [57]. The comparison between the experimental EMG and the reconstructed EMG in Fig. 6d reveals that the framework usually underestimates some muscle activities, which may be due to these factors. Although it may be possible to consider stabilizing synergies (ones that produce zero task space force), this idea was not investigated in this paper.

4.3 Acquiring the synergies and the relation to motor learning

Muscle synergies, if they exist, are probably formed either through evolution (prior to the movement) or practice (concurrent with the movement). In this paper, an off-line learning method was implemented; however, this assumption does not affect the generalizability of the motor control framework. The synergies should be structured to result in the best performance in doing a task. We made our arguments in the simulations based on physiological effort minimization, because a well-practised motion (such as reaching) is physiologically efficient. Furthermore, it was shown in [67] that muscle synergies obtained from the optimal activation date resembles those obtained from EMG data.

Another important performance index that needs to be addressed is the robustness/generalizability in novel conditions (as observed in [68]). In this research, the synergies were assumed to be task-specific, which raises the question whether new synergies are formed for a new task, or if the general-purpose synergies would still be used.

We previously showed [45] that for a 1D task space (e.g. rotating a steering wheel), two task-specific synergies are enough to achieve the optimal control performance; for the more general 3D task, five synergies only approximate the optimal results. One may link the gradual performance improvement observed during motor learning to this task-specificity. Our thought regarding motor learning is that the nervous system may initially try to control a novel task (e.g. playing violin with a bow, which has very specific task requirements) with the available synergy sets (e.g. 3D reaching synergies). As the task is repeated, the nervous system explores the neighbouring solutions, and eventually learns a new synergy set (as well as a fine-tuned task space controller), until a "*good-enough*" solution is reached [69].

4.4 Applications of the framework

There are important applications for the proposed motor control framework. As was shown, such a *controller* is a necessity in many musculoskeletal simulations. The proposed motor control model can be a viable tool for the fast feedback motion control of a musculoskeletal system with near-optimal performance. Moreover, it has the advantage of being generalizable to control any system. One example of predictive musculoskeletal simulation was presented in this paper. More example simulations with different task spaces are available for the interested reader in [49]. The presented framework may also be

used as a computational tool to investigate motor control theories.

In model-based control of prosthetic and orthotic devices, it is essential to have a model that behaves similarly to the human motor control system. Control of limb movement via functional electrical stimulation (FES) of the muscles requires a real-time optimal feedback controller that can handle the complexities of the human musculoskeletal system [70, 71].

In another application, synergy-based myoelectric control of assistive devices has been shown to be a promising approach [72, 73, 74], and the task/synergy relationship presented in this motor control framework seems well-suited for such purposes.

5 Conclusions

In this paper we presented a feedback motor control framework based on muscle synergies. The hierarchical structure of the framework allowed for fast feedback control of the movements, by separating the control of the task space variables from the complexities of the musculoskeletal system. The bridge between the task and muscle spaces was a mapping that converted the force signals in the task space to muscle activation. This mapping used posture-dependent muscle synergies and the corresponding basis vectors for the force decomposition. We showed two separate sets of results; the experimental results showed acceptable performance of the method (approximately 70% accuracy), while the simulation results showed strong potential of the proposed motor control framework for the fast and near-optimal feedback control of musculoskeletal systems.

Acknowledgement

The authors wish to acknowledge the Natural Sciences and Engineering Research Council of Canada (NSERC) and the Canada Research Chairs program for funding support of this study. The authors also wish to thank Quanser Inc. for the donation of the rehabilitation robot used in this study.

References

[1] Bernstein, M., 1967. *The co-ordination and regulation of movements.*, 1st ed. Pergamon Press, Oxford, New York.

[2] Morasso, P., 1981. "Spatial control of arm movements". *Experimental Brain Research,* **42**, pp. 223–227.

[3] Scholz, J., and Schöner, G., 1999. "The uncontrolled manifold concept: identifying control variables for a functional task.". *Experimental Brain Research.,* **126**(3), jun, pp. 289–306.

[4] Georgopoulos, A. P., Schwartz, A. B., and Kettner, R. E., 1986. "Neuronal population coding of movement direction". *Science,* **233**(1986), pp. 1416–1419.

[5] Georgopoulos, A. P., Kettner, R. E., and Schwartz, a. B., 1988. "Primate motor cortex and free arm movements to visual targets in three-dimensional space. II. Coding of the direction of movement by a neuronal population". *Journal of Neuroscience,* **8**(8), pp. 2928–2937.

[6] Schwartz, A. B., Kettner, R. E., and Georgopoulos, A. P., 1988. "Primate motor cortex and free arm movements to visual targets in three-dimensional space. I. Relations between single cell discharge and direction of movement". *Journal of Neuroscience,* **8**(August), pp. 2913–2927.

[7] Lillicrap, T. P., and Scott, S. H., 2013. "Preference Distributions of Primary Motor Cortex Neurons Reflect Control Solutions Optimized for Limb Biomechanics". *Neuron,* **77**(1), pp. 168–179.

[8] Erdemir, A., McLean, S., Herzog, W., and van den Bogert, A. J., 2007. "Model-based estimation of muscle forces exerted during movements". *Clinical Biomechanics (Bristol, Avon),* **22**(2), feb, pp. 131–154.

[9] Meyer, A. J., Eskinazi, I., Jackson, J. N., Rao, A. V., Patten, C., and Fregly, B. J., 2016. "Muscle Synergies Facilitate Computational Prediction of Subject-Specific Walking Motions". *Frontiers in Bioengineering and Biotechnology,* **4**, oct, p. 77.

[10] Sharif Shourijeh, M., Smale, K. B., Potvin, B. M., and Benoit, D. L., 2016. "A forward-muscular inverse-skeletal dynamics framework for human musculoskeletal simulations". *Journal of Biomechanics,* **49**(9), pp. 1718–1723.

[11] Walter, J. P., Kinney, A. L., Banks, S. a., D'Lima, D. D., Besier, T. F., Lloyd, D. G., and Fregly, B. J., 2014. "Muscle synergies may improve optimization prediction of knee contact forces during walking.". *Journal of Biomechanical Engineering,* **136**(2), p. 021031.

[12] Neptune, R. R., Clark, D. J., and Kautz, S. A., 2009. "Modular control of human walking: a simulation study.". *Journal of Biomechanics,* **42**(9), jun, pp. 1282–7.

[13] Anderson, F. C., and Pandy, M. G., 2001. "Dynamic Optimization of Human Walking". *Journal of Biomechanical Engineering,* **123**(5), p. 381.

[14] Sharif Razavian, R., Mehrabi, N., and McPhee, J., 2015. "A Neuronal Model of Central Pattern Generator to Account for Natural Motion Variation". *Journal of Computational and Nonlinear Dynamics,* **11**(2), aug, p. 021007.

[15] Berniker, M., Jarc, A., Bizzi, E., and Tresch, M. C., 2009. "Simplified and effective motor control based on muscle synergies to exploit musculoskeletal dynamics.". *Proceedings of the National Academy of Sciences of the United States of America,* **106**(18), may, pp. 7601–6.

[16] Jagodnik, K. M., Blana, D., van den Bogert, A. J., and Kirsch, R. F., 2015. "An optimized proportional-derivative controller for the human upper extremity with gravity". *Journal of Biomechanics,* **48**(13), pp. 3701–3709.

[17] Jagodnik, K. M., and van den Bogert, A. J., 2010. "Optimization and evaluation of a proportional derivative controller for planar arm movement". *Journal of Biomechanics,* **43**(6), apr, pp. 1086–1091.

[18] Jagodnik, K. M., Thomas, P. S., Van Den Bogert, A. J., Branicky, M. S., and Kirsch, R. F., 2017. "Training an Actor-Critic Reinforcement Learning Controller for Arm Movement Using Human-Generated Rewards". *IEEE Transactions on Neural Systems and Rehabilitation Engineering,* **25**(10), pp. 1892–1905.

[19] Fu, K. C. D., Libera, F. D., and Ishiguro, H., 2015. "Extracting motor synergies from random movements for low-dimensional task-space control of musculoskeletal robots". *Bioinspiration & Biomimetics,* **10**(5), p. 056016.

[20] Park, H., and Durand, D. M., 2008. "Motion control of musculoskeletal systems with redundancy.". *Biological Cybernetics,* **99**(6), dec, pp. 503–16.

[21] Blana, D., Kirsch, R. F., and Chadwick, E. K., 2009. "Combined feedforward and feedback control of a redundant, nonlinear, dynamic musculoskeletal system". *Medical & Biological Engineering & Computing,* **47**(5), apr, pp. 533–542.

[22] Tresch, M. C., and Jarc, A., 2009. "The case for and against muscle synergies". *Current Opinion in Neurobiology,* **19**(6), pp. 601–607.

[23] Hilt, P. M., Delis, I., Pozzo, T., and Berret, B., 2018. "Space-by-time modular decomposition effectively describes whole-body muscle activity during upright reaching in various directions". *Frontiers in Computational Neuroscience,* **12**(April), pp. 1–19.

[24] Sharif Shourijeh, M., Flaxman, T. E., and Benoit, D. L., 2016. "An approach for improving repeatability and reliability of non-negative matrix factorization for muscle synergy analysis". *Journal of Electromyography and Kinesiology,* **26**, feb, pp. 36–43.

[25] Smale, K. B., Sharif Shourijeh, M., and Benoit, D. L., 2016. "Use of muscle synergies and wavelet transforms to identify fatigue during squatting". *Journal of Electromyography and Kinesiology,* **28**, pp. 158–166.

[26] Kutch, J. J., Kuo, A. D., Bloch, A. M., and Rymer, W. Z., 2008. "Endpoint Force Fluctuations Reveal Flexible Rather Than Synergistic Patterns of Muscle Cooperation". *Journal of Neurophysiology,* **100**(5), pp. 2455–2471.

[27] D'Avella, A., Portone, A., Fernandez, L., and Lacquaniti, F., 2006. "Control of fast-reaching movements by muscle synergy combinations.". *The Journal of neuroscience : the official journal of the Society for Neuroscience,* **26**(30), jul, pp. 7791–810.

[28] Ivanenko, Y. P., Poppele, R. E., and Lacquaniti, F., 2004. "Five basic muscle activation patterns account for muscle activity during human locomotion". *Journal of Physiology,* **556**(1), pp. 267–282.

[29] Berger, D. J., Gentner, R., Edmunds, T., Pai, D. K., and D'Avella, A., 2013. "Differences in Adaptation Rates after Virtual Surgeries Provide Direct Evidence for Modularity". *Journal of Neuroscience,* **33**(30), pp. 12384–12394.

[30] Dominici, N., Ivanenko, Y. P., Cappellini, G., D'Avella, A., Mond??, V., Cicchese, M., Fabiano, A., Silei, T., Di Paolo, A., Giannini, C., Poppele, R. E., and Lacquaniti, F., 2011. "Locomotor primitives in newborn babies and their development".

Science, **334**(6058), pp. 997–999.

[31] Zariffa, J., Steeves, J., and Pai, D. K., 2012. "Changes in hand muscle synergies in subjects with spinal cord injury: Characterization and functional implications". *Journal of Spinal Cord Medicine,* **35**(5), pp. 310–318.

[32] Clark, D. J., Ting, L. H., Zajac, F. E., Neptune, R. R., and Kautz, S. A., 2010. "Merging of Healthy Motor Modules Predicts Reduced Locomotor Performance and Muscle Coordination Complexity Post-Stroke". *Journal of Neurophysiology,* **103**(2), pp. 844–857.

[33] Steele, K. M., Rozumalski, A., and Schwartz, M. H., 2015. "Muscle synergies and complexity of neuromuscular control during gait in cerebral palsy". *Developmental Medicine & Child Neurology*, pp. n/a–n/a.

[34] Overduin, S. A., D'Avella, A., Roh, J., and Bizzi, E., 2008. "Modulation of Muscle Synergy Recruitment in Primate Grasping". *Journal of Neuroscience,* **28**(4), pp. 880–892.

[35] Bizzi, E., Cheung, V. C. K., D'Avella, A., Saltiel, P., and Tresch, M. C., 2008. "Combining modules for movement.". *Brain Research Reviews,* **57**(1), jan, pp. 125–33.

[36] Cheung, V. C. K., D'Avella, A., Tresch, M. C., and Bizzi, E., 2005. "Central and sensory contributions to the activation and organization of muscle synergies during natural motor behaviors.". *The Journal of Neuroscience : the Official Journal of the Society for Neuroscience,* **25**(27), jul, pp. 6419–34.

[37] Hart, C. B., and Giszter, S. F., 2004. "Modular premotor drives and unit bursts as primitives for frog motor behaviors.". *The Journal of neuroscience : the official journal of the Society for Neuroscience,* **24**(22), jun, pp. 5269–82.

[38] Saltiel, P., Wyler-Duda, K., D'Avella, A., Tresch, M. C., and Bizzi, E., 2001. "Muscle synergies encoded within the spinal cord: evidence from focal intraspinal NMDA iontophoresis in the frog.". *Journal of neurophysiology,* **85**(2), feb, pp. 605–19.

[39] Tresch, M. C., Saltiel, P., and Bizzi, E., 1999. "The construction of movement by the spinal cord". *Nature Neuroscience,* **2**(2), feb, pp. 162–167.

[40] Sohn, M. H., and Ting, L. H., 2016. "Suboptimal muscle synergy activation patterns generalize their motor function across postures". *Frontiers in Computational Neuroscience,* **10**(February), pp. 1–15.

[41] Ting, L. H., and McKay, J. L., 2007. "Neuromechanics of muscle synergies for posture and movement.". *Current Opinion in Neurobiology,* **17**(6), dec, pp. 622–8.

[42] Torres-Oviedo, G., Macpherson, J. M., and Ting, L. H., 2006. "Muscle Synergy Organization Is Robust Across a Variety of Postural Perturbations". *Journal of Neurophysiology,* **96**(3), sep, pp. 1530–1546.

[43] Ting, L. H., and Macpherson, J. M., 2004. "Ratio of Shear to Load Ground-Reaction Force May Underlie the Directional Tuning of the Automatic Postural Response to Rotation and Translation". *Journal of Neurophysiology,* **92**(2), aug, pp. 808–823.

[44] Lockhart, D. B., and Ting, L. H., 2007. "Optimal sensorimotor transformations for balance.". *Nature Neuroscience,* **10**(10), oct, pp. 1329–36.

[45] Sharif Razavian, R., Mehrabi, N., and McPhee, J., 2015. "A model-based approach to predict muscle synergies using optimization: application to feedback control". *Frontiers in Computational Neuroscience,* **9**(October), oct, pp. 1–13.

[46] Kargo, W. J., Ramakrishnan, A., Hart, C. B., Rome, L. C., and Giszter, S. F., 2010. "A simple experimentally based model using proprioceptive regulation of motor primitives captures adjusted trajectory formation in spinal frogs.". *Journal of neurophysiology,* **103**(1), jan, pp. 573–90.

[47] Alessandro, C., Carbajal, J. P., and D'Avella, A., 2014. "A computational analysis of motor synergies by dynamic response decomposition". *Frontiers in Computational Neuroscience,* **7**(January), pp. 1–20.

[48] Sharif Razavian, R., Ghannadi, B., and McPhee, J., 2018. "On the relationship between muscle synergies and redundant degrees of freedom in musculoskeletal systems". *Frontiers in Computational Neuroscience (submitted)*.

[49] Sharif Razavian, R., 2017. "A Human Motor Control Framework based on Muscle Synergies". Phd thesis, University of Waterloo.

[50] Sharif Razavian, R., and McPhee, J., 2016. "A motor control framework for the fast control of a 3D musculoskeletal arm motion using muscle synergy". In The 4th Joint International Conference on Multibody System Dynamics.

[51] Boettcher, C. E., Ginn, K. A., and Cathers, I., 2008. "Standard maximum isometric voluntary contraction tests for normalizing shoulder muscle EMG". *Journal of Orthopaedic Research,* **26**(12), pp. 1591–1597.

[52] Lee, D. D., and Seung, H. S., 2001. "Algorithms for non-negative matrix factorization". *Advances in Neural Information Processing Systems,* **13**(1), pp. 556–562.

[53] Tresch, M. C., Cheung, V. C. K., and D'Avella, A., 2006. "Matrix factorization algorithms for the identification of muscle synergies: evaluation on simulated and experimental data sets.". *Journal of neurophysiology,* **95**(4), apr, pp. 2199–212.

[54] Roh, J., Rymer, W. Z., and Beer, R. F., 2012. "Robustness of muscle synergies underlying three-dimensional force generation at the hand in healthy humans". *Journal of Neurophysiology,* **107**(8), pp. 2123–2142.

[55] de Rugy, A., Loeb, G. E., and Carroll, T. J., 2013. "Are muscle synergies useful for neural control?". *Frontiers in Computational Neuroscience,* **7**(March), pp. 1–13.

[56] Mehrabi, N., Sharif Razavian, R., and McPhee, J., 2015. "Steering disturbance rejection using a physics-based neuromusculoskeletal driver model". *Vehicle System Dynamics,* **53**(10), oct, pp. 1393–1415.

[57] Thelen, D. G., 2003. "Adjustment of Muscle Mechanics Model Parameters to Simulate Dynamic Contractions in Older Adults". *Journal of Biomechanical Engineering,* **125**(1), p. 70.

[58] Mehrabi, N., Sharif Razavian, R., Ghannadi, B., and McPhee, J., 2017. "Predictive Simulation of Reaching Moving Targets Using Nonlinear Model Predictive Control". *Frontiers in Computational Neuroscience,* **10**(143), jan.

[59] Sartori, M., Gizzi, L., Lloyd, D. G., and Farina, D., 2013. "A musculoskeletal model of human locomotion driven by a low dimensional set of impulsive excitation primitives.". *Frontiers in computational neuroscience,* **7**(June), p. 79.

[60] Moran, D., and Schwartz, A. B., 1999. "Motor Cortical Representation of Speed and Direction During Reaching". *Journal of Neurophysiology,* **82**, pp. 2676–2692.

[61] Boline, J., and Ashe, J., 2005. "On the relations between single cell activity in the motor cortex and the direction and magnitude of three-dimensional dynamic isometric force". *Experimental Brain Research,* **167**(2), nov, pp. 148–159.

[62] Kettner, R. E., Schwartz, a. B., and Georgopoulos, A. P., 1988. "Primate motor cortex and free arm movements to visual targets in three-dimensional space. III. Positional gradients and population coding of movement direction from various movement origins". *Journal of Neuroscience,* **8**(8), pp. 2938–2947.

[63] Ashe, J., and Georgopoulos, A. P., 1994. "Movement Parameters and Neural Activity in Motor Cortex and Area 5". *Cerebral Cortex,* **4**(6), pp. 590–600.

[64] Todorov, E., and Jordan, M. I., 2002. "A Minimal Intervention Principle for Coordinated Movement". In Advances in Neural Information Processing Systems: Proceedings of the 2002 Conference, pp. 27–34.

[65] de Rugy, A., Loeb, G. E., and Carroll, T. J., 2012. "Muscle Coordination Is Habitual Rather than Optimal". *Journal of Neuroscience,* **32**(21), pp. 7384–7391.

[66] Krishnamoorthy, V., Scholz, J. P., and Latash, M. L., 2007. "The use of flexible arm muscle synergies to perform an isometric stabilization task". *Clinical Neurophysiology,* **118**(3), pp. 525–537.

[67] Steele, K. M., Tresch, M. C., and Perreault, E. J., 2013. "The number and choice of muscles impact the results of muscle synergy analyses.". *Frontiers in computational neuroscience,* **7**(August), p. 105.

[68] Gentner, R., Edmunds, T., Pai, D. K., and D'Avella, A., 2013. "Robustness of muscle synergies during visuomotor adaptation.". *Frontiers in Computational Neuroscience,* **7**(September), p. 120.

[69] Loeb, G. E., 2012. "Optimal isn't good enough.". *Biological cybernetics,* **106**(11-12), dec, pp. 757–65.

[70] Sharif Razavian, R., Ghannadi, B., and McPhee, J., 2017. "Feedback control of functional electrical stimulation for arbitrary upper extremity movements". In 2017 International Conference on Rehabilitation Robotics (ICORR), IEEE, pp. 1451–1456.

[71] Sharif Razavian, R., Ghannadi, B., Mehrabi, N., Charlet, M., and McPhee, J., 2018. "Feedback Control of Functional Electrical Stimulation for 2D Arm Reaching Movements.". *IEEE transactions on neural systems and rehabilitation engineering : a publication of the IEEE Engineering in Medicine and Biology Society*, jul, pp. 1–1.

[72] Berger, D. J., and D'Avella, A., 2014. "Effective force control by muscle synergies.". *Frontiers in computational neuroscience,* **8**(April), p. 46.

[73] Jiang, N., Rehbaum, H., Vujaklija, I., Graimann, B., and Farina, D., 2014. "Intuitive, online, simultaneous, and proportional myoelectric control over two degrees-of-freedom in upper limb amputees". *IEEE Transactions on Neural Systems and Rehabilitation Engineering,* **22**(3), pp. 501–510.

[74] Muceli, S., Jiang, N., and Farina, D., 2014. "Extracting signals robust to electrode number and shift for online simultaneous and proportional myoelectric control by factorization algorithms". *IEEE Transactions on Neural Systems and Rehabilitation Engineering,* **22**(3), pp. 623–633.

Supplementary Materials: Detailed experimental results

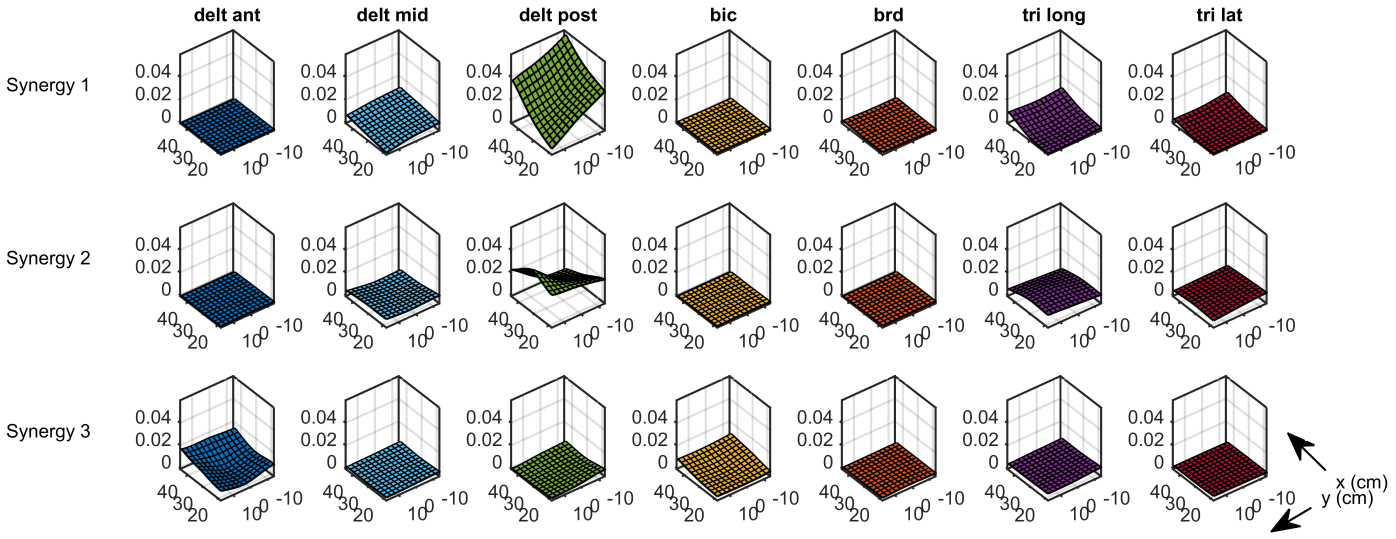

(a)

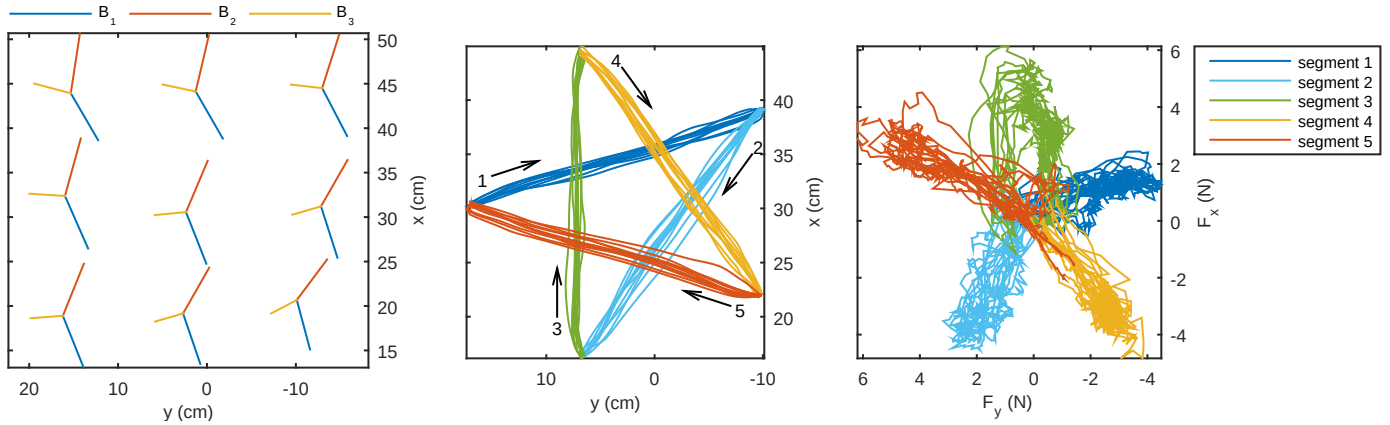

(b) (c)

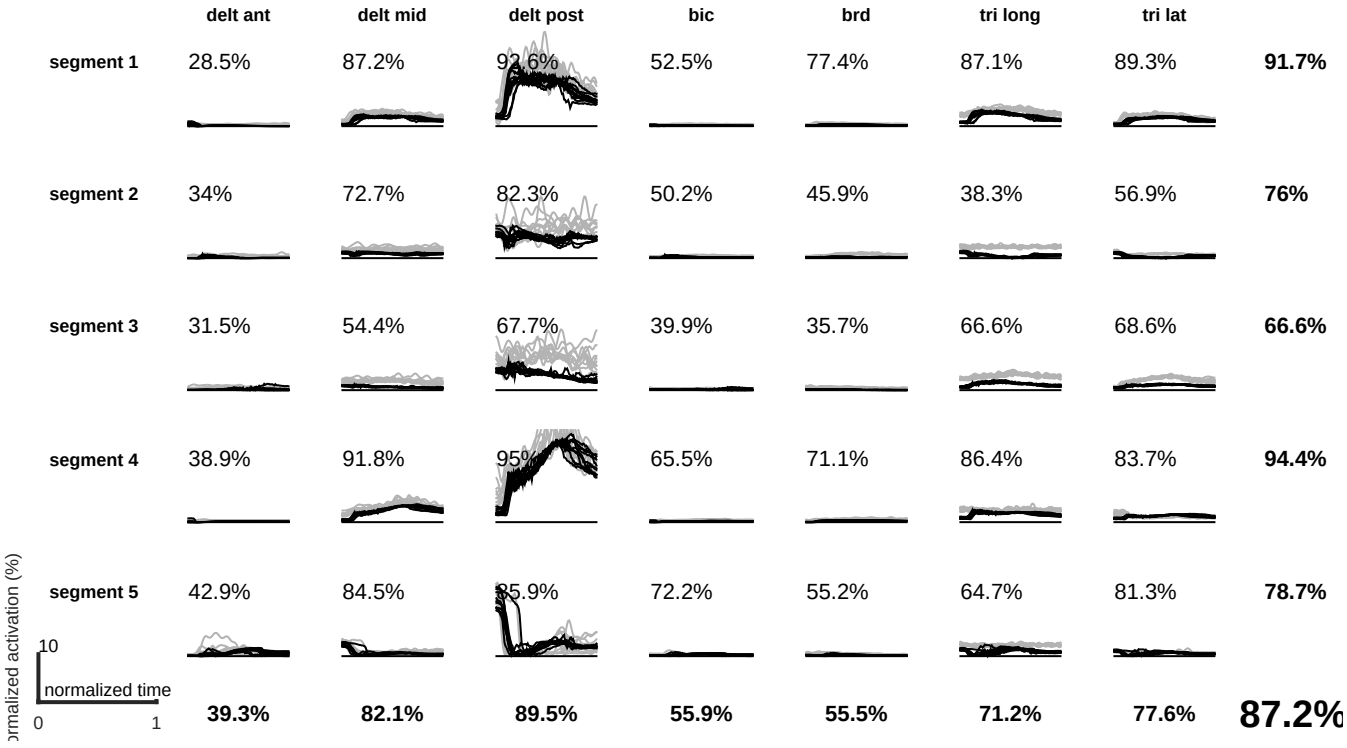

(d)

Sup. Fig. 1: Subject #1's results. (a) Detailed muscle activity levels in the synergies (b) basis vectors (c) motion trials (d) EMG measurements and reconstruction.

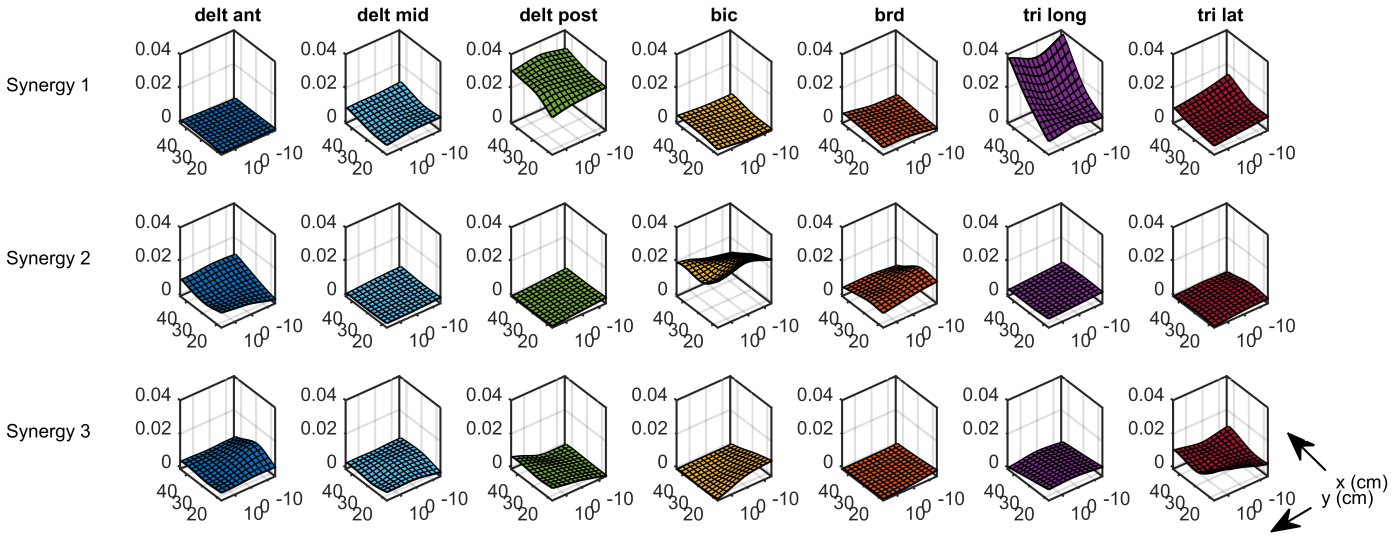

(a)

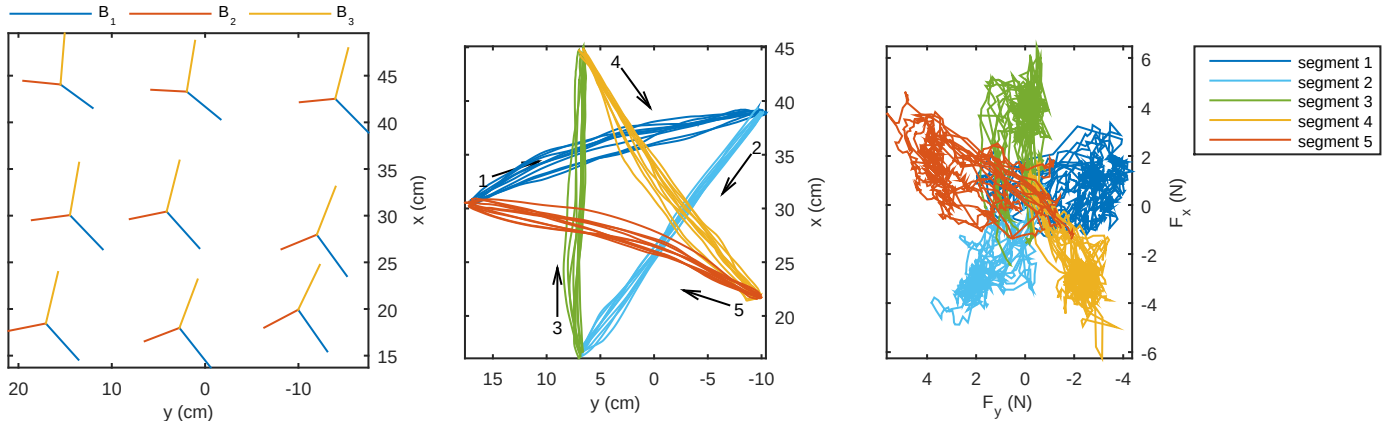

(b) (c)

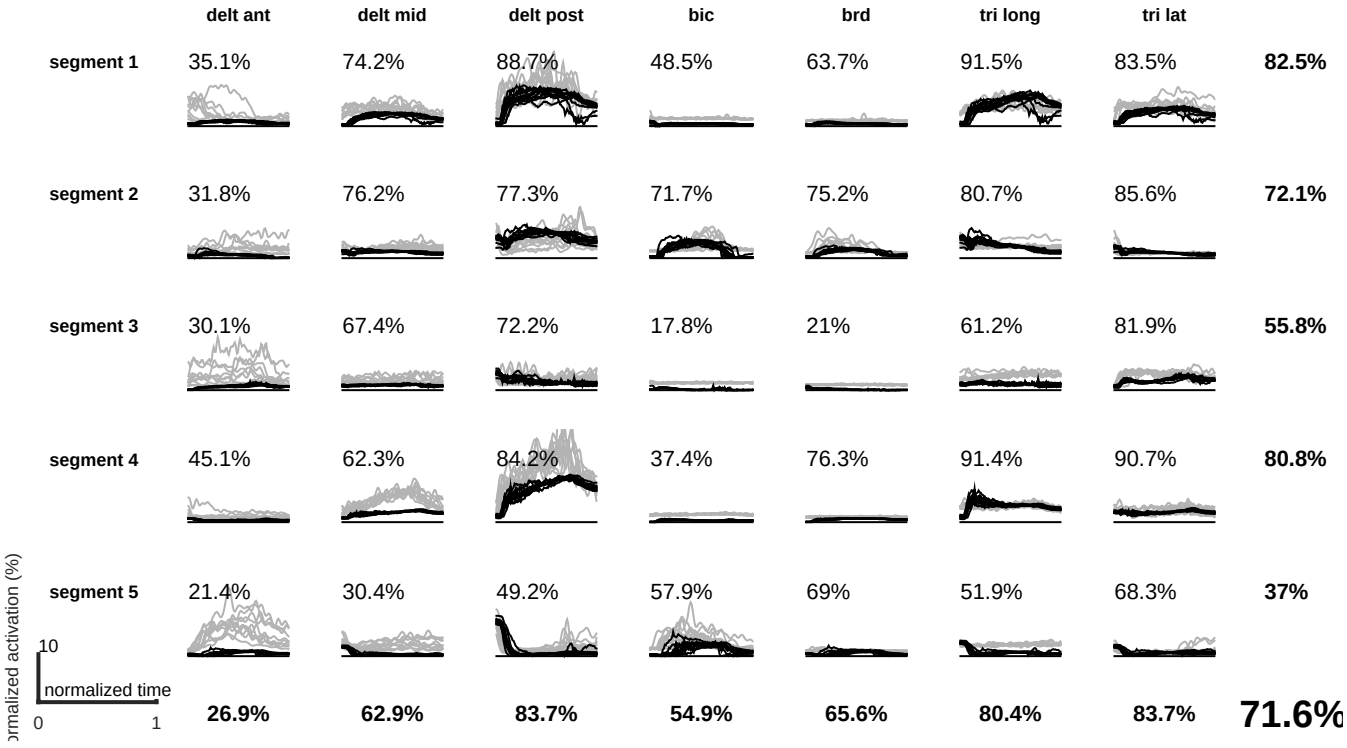

(d)

Sup. Fig. 2: Subject #2's results. (a) Detailed muscle activity levels in the synergies (b) basis vectors (c) motion trials (d) EMG measurements and reconstruction.

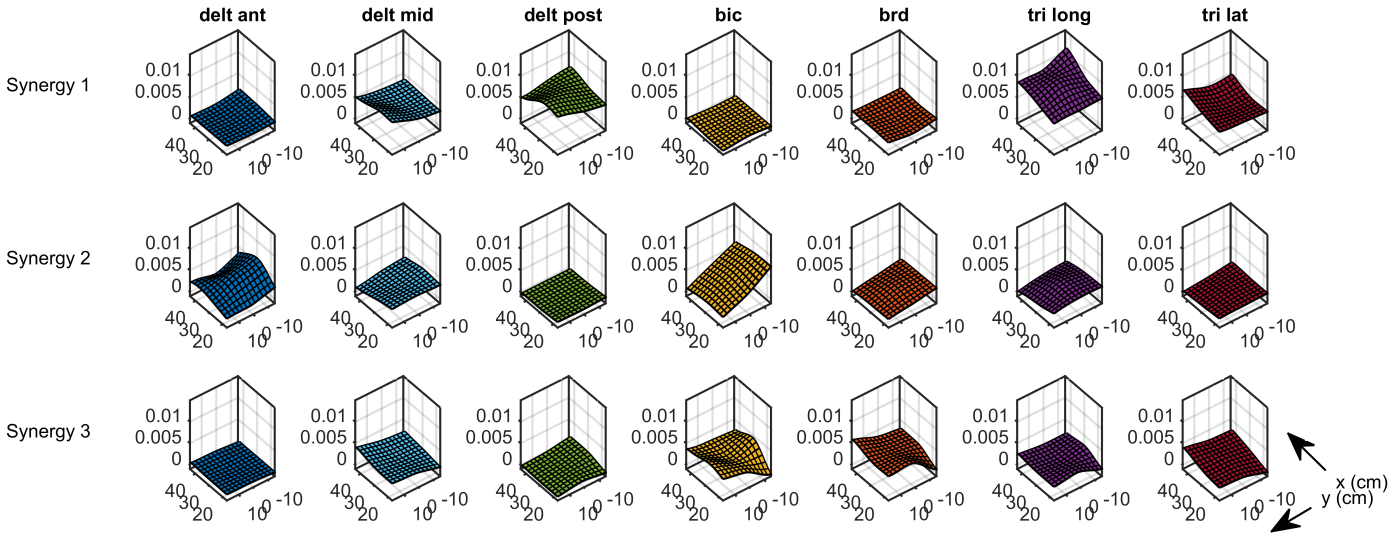

(a)

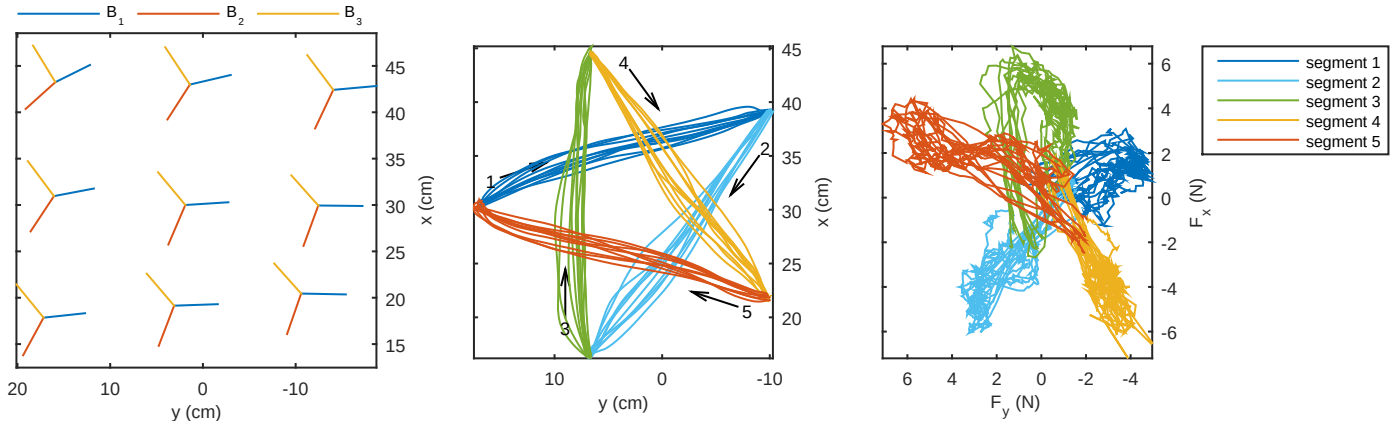

(b) (c)

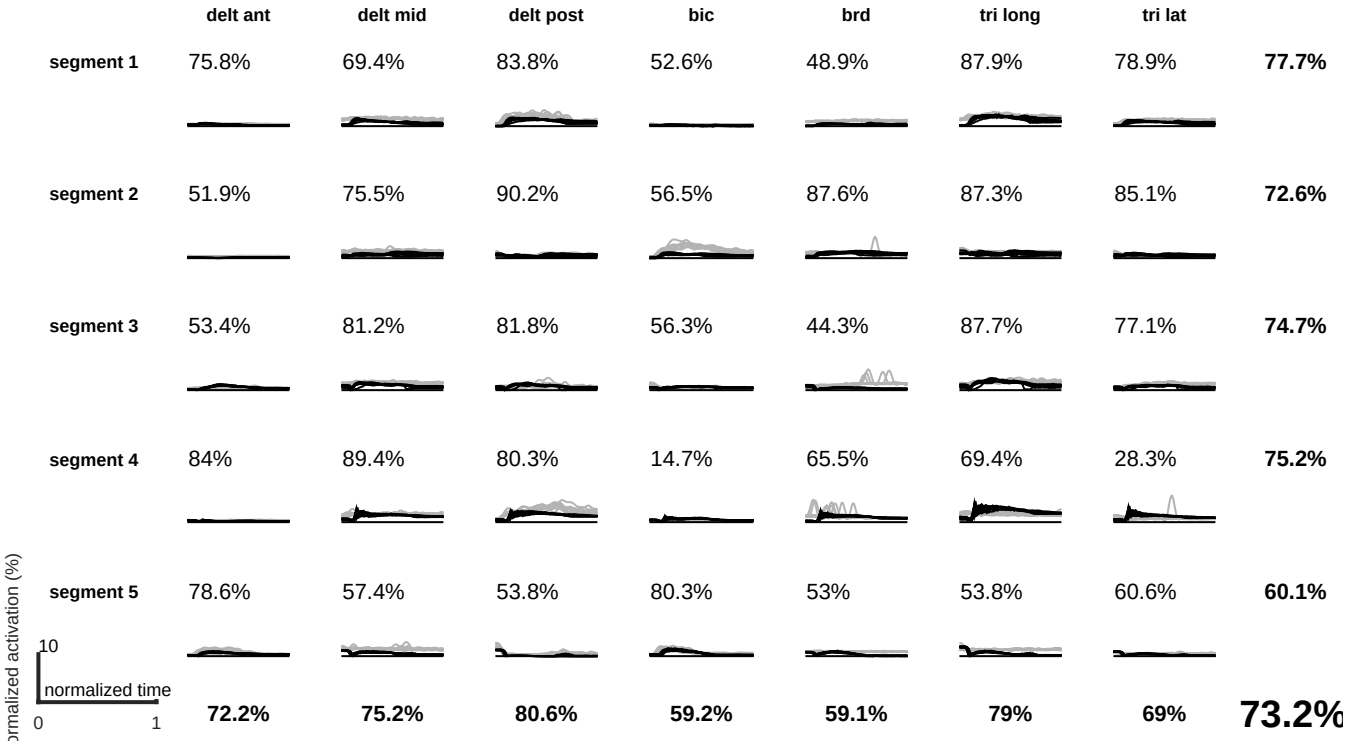

(d)

Sup. Fig. 3: Subject #3's results. (a) Detailed muscle activity levels in the synergies (b) basis vectors (c) motion trials (d) EMG measurements and reconstruction.

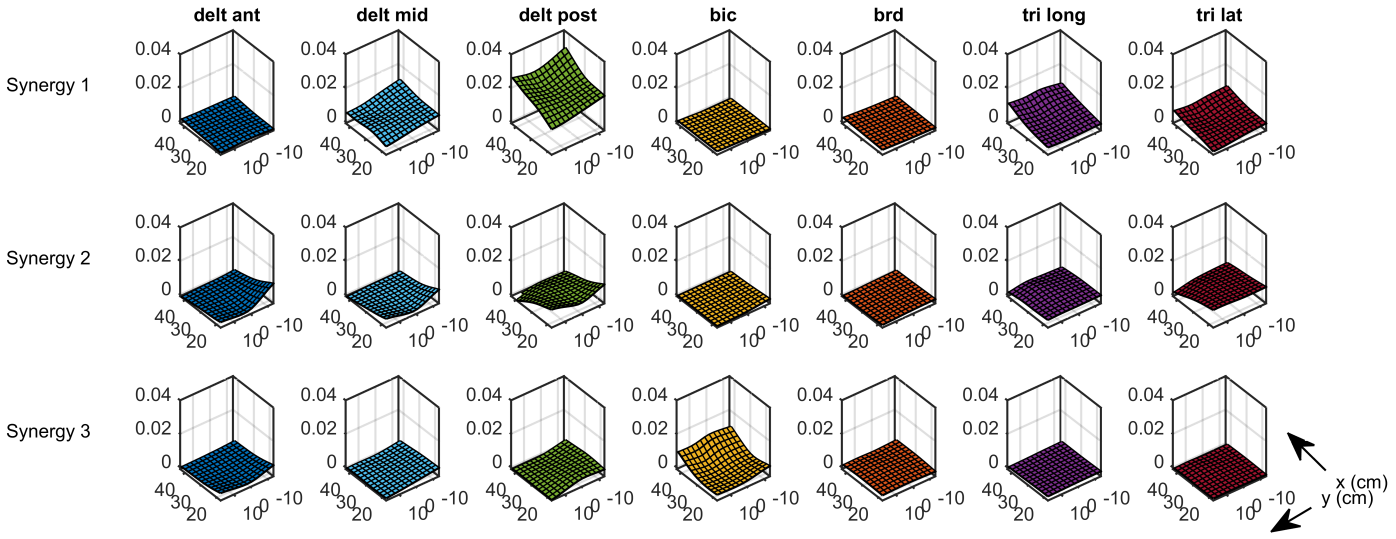

(a)

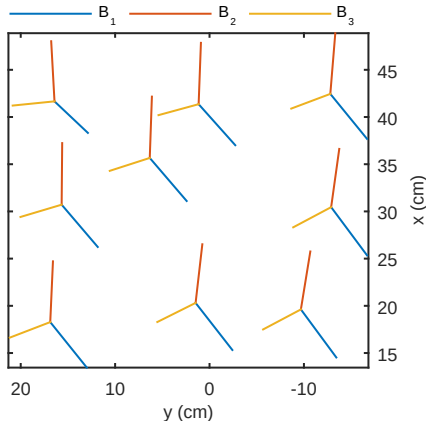

(b)

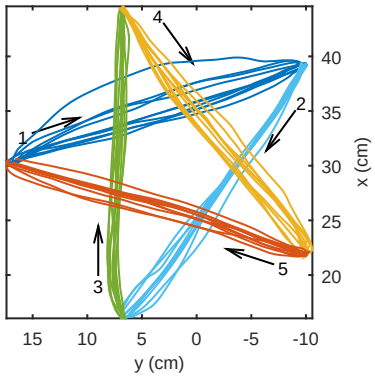

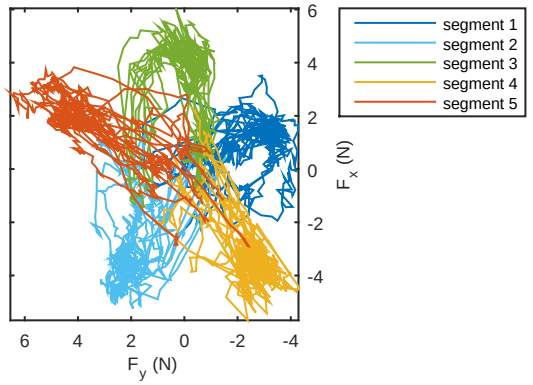

(c)

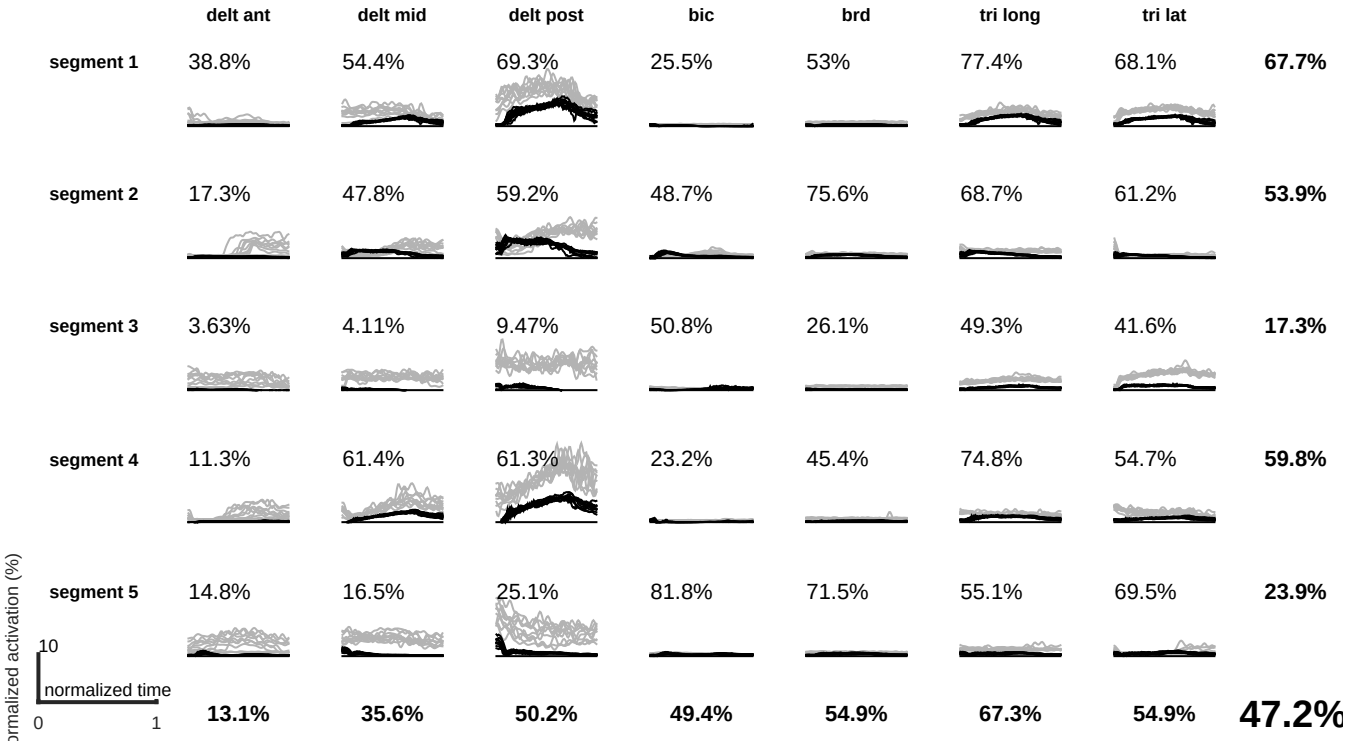

(d)

Sup. Fig. 4: Subject #4's results. (a) Detailed muscle activity levels in the synergies (b) basis vectors (c) motion trials (d) EMG measurements and reconstruction.

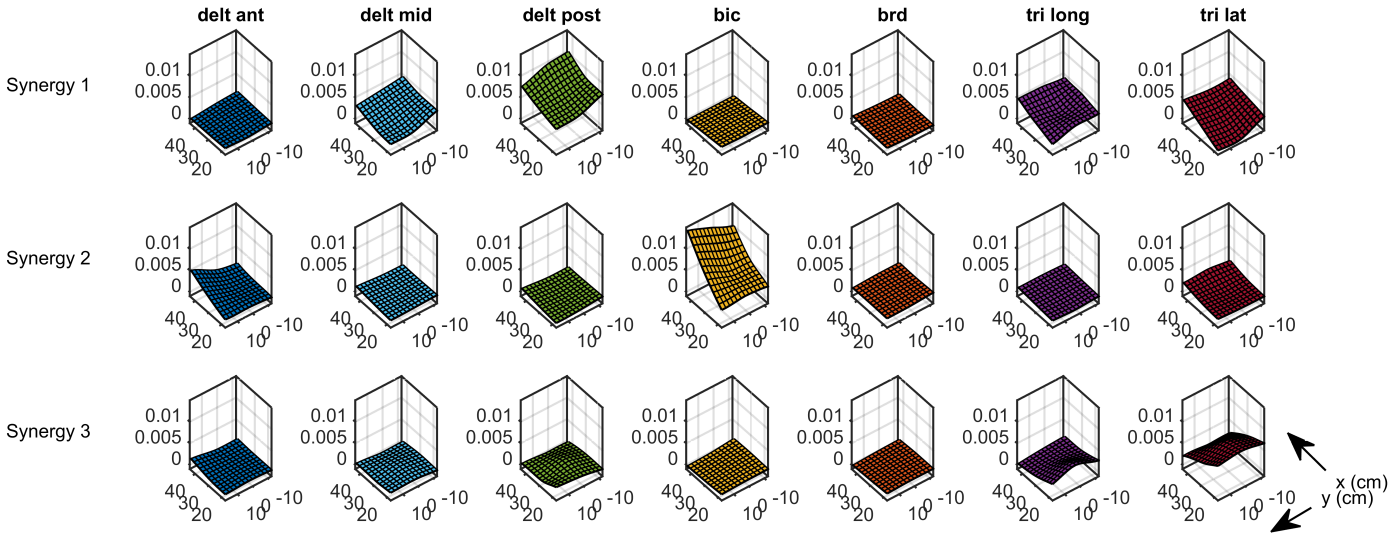

(a)

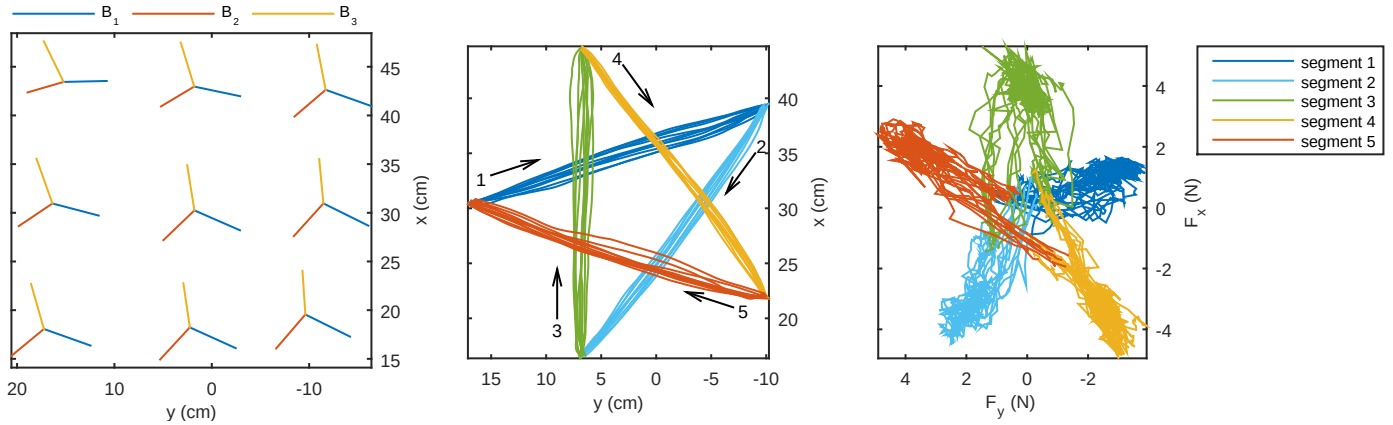

(b) (c)

(d)

Sup. Fig. 5: Subject #5's results. (a) Detailed muscle activity levels in the synergies (b) basis vectors (c) motion trials (d) EMG measurements and reconstruction.

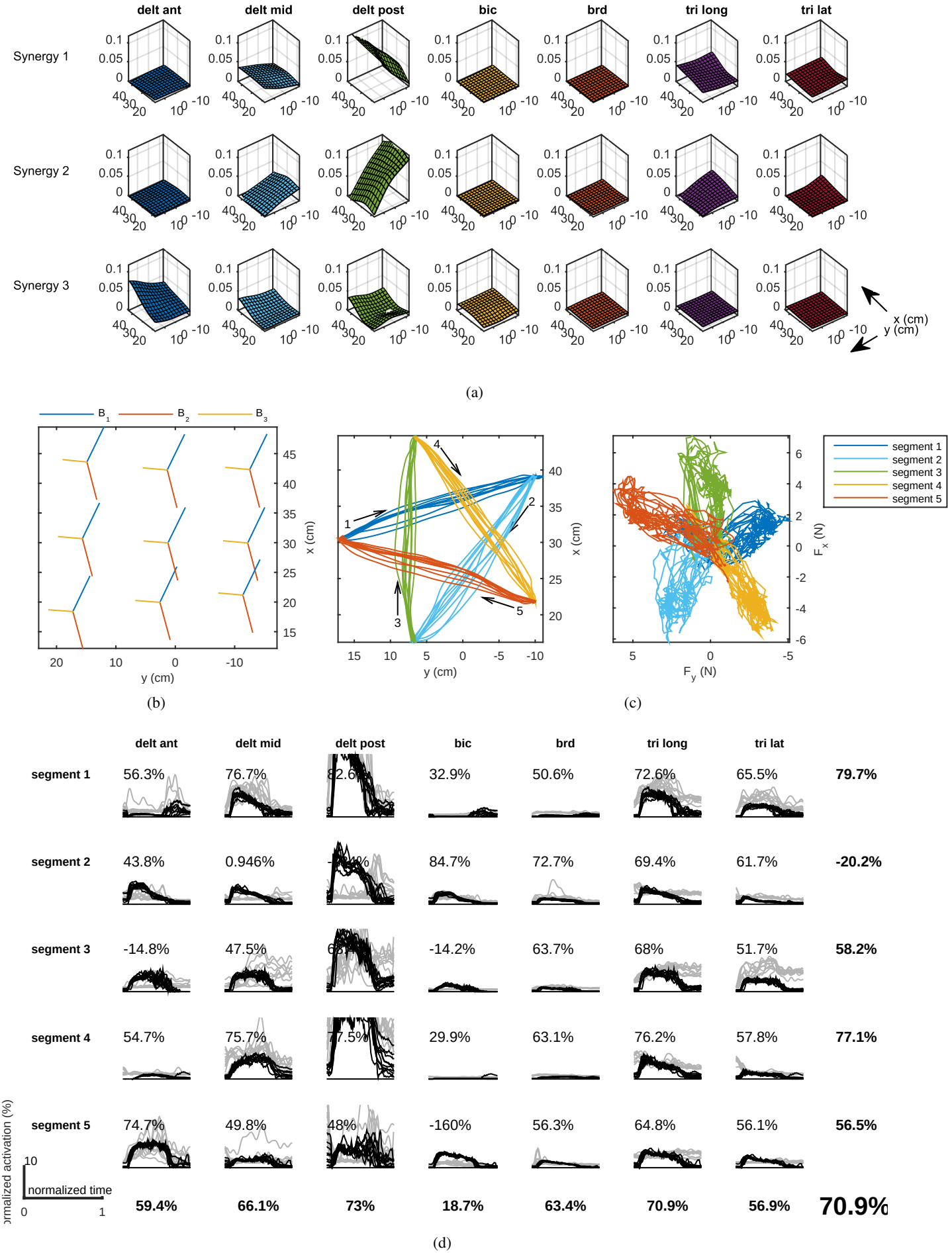

Sup. Fig. 6: Subject #6's results. (a) Detailed muscle activity levels in the synergies (b) basis vectors (c) motion trials (d) EMG measurements and reconstruction.

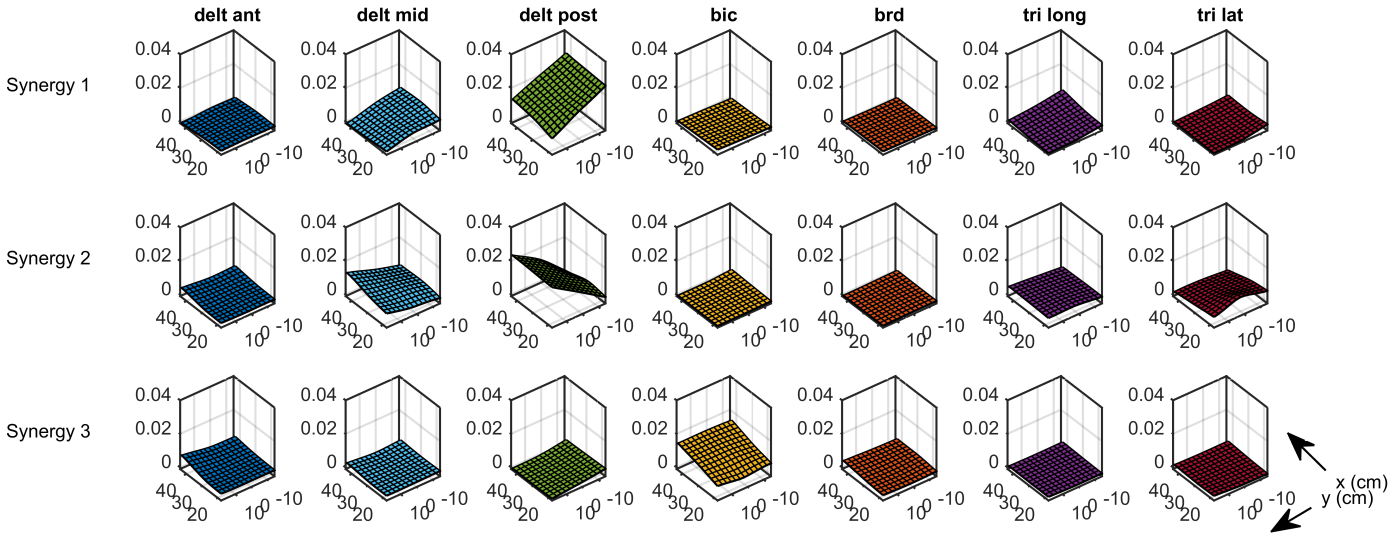

(a)

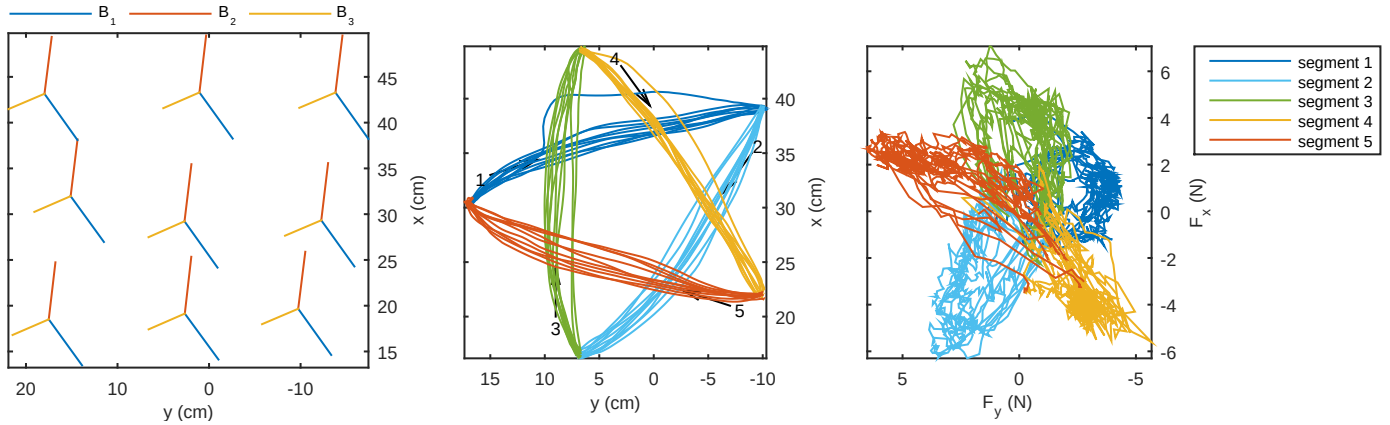

(b) (c)

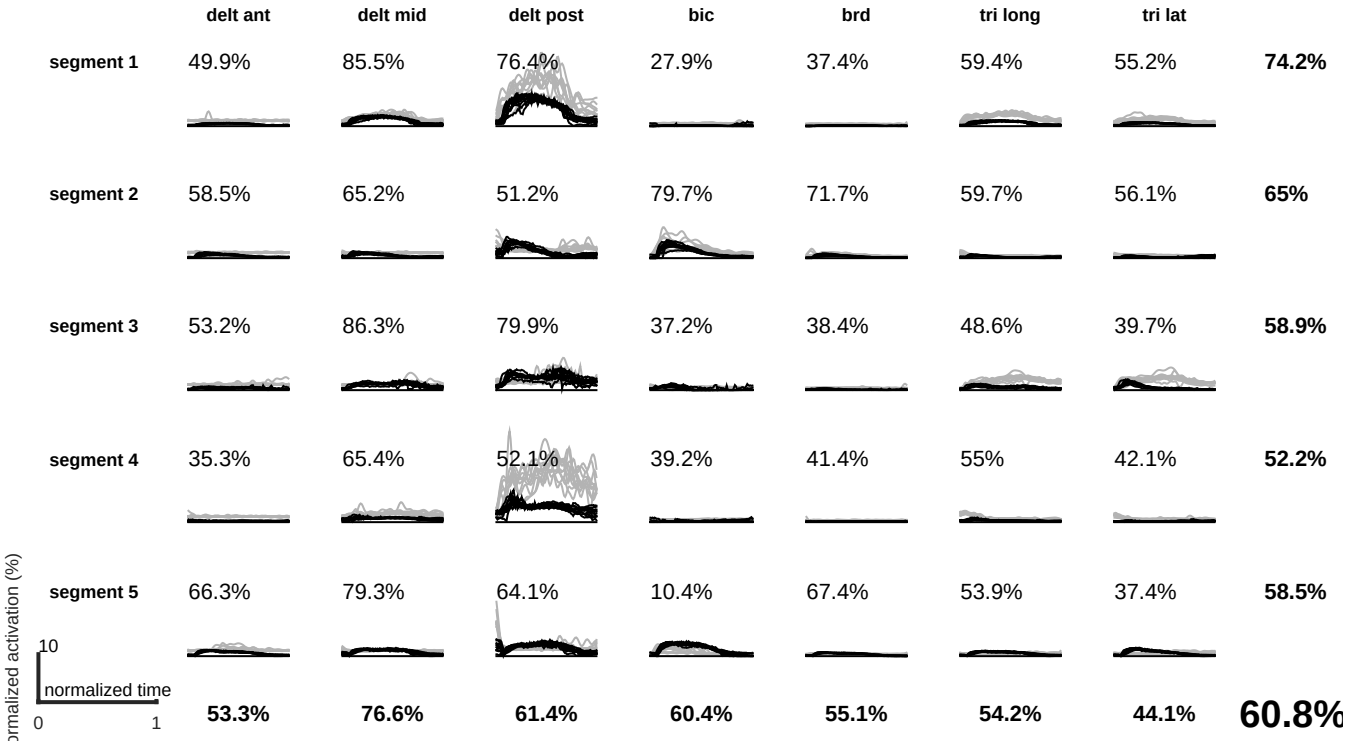

(d)

Sup. Fig. 7: Subject #7's results. (a) Detailed muscle activity levels in the synergies (b) basis vectors (c) motion trials (d) EMG measurements and reconstruction.

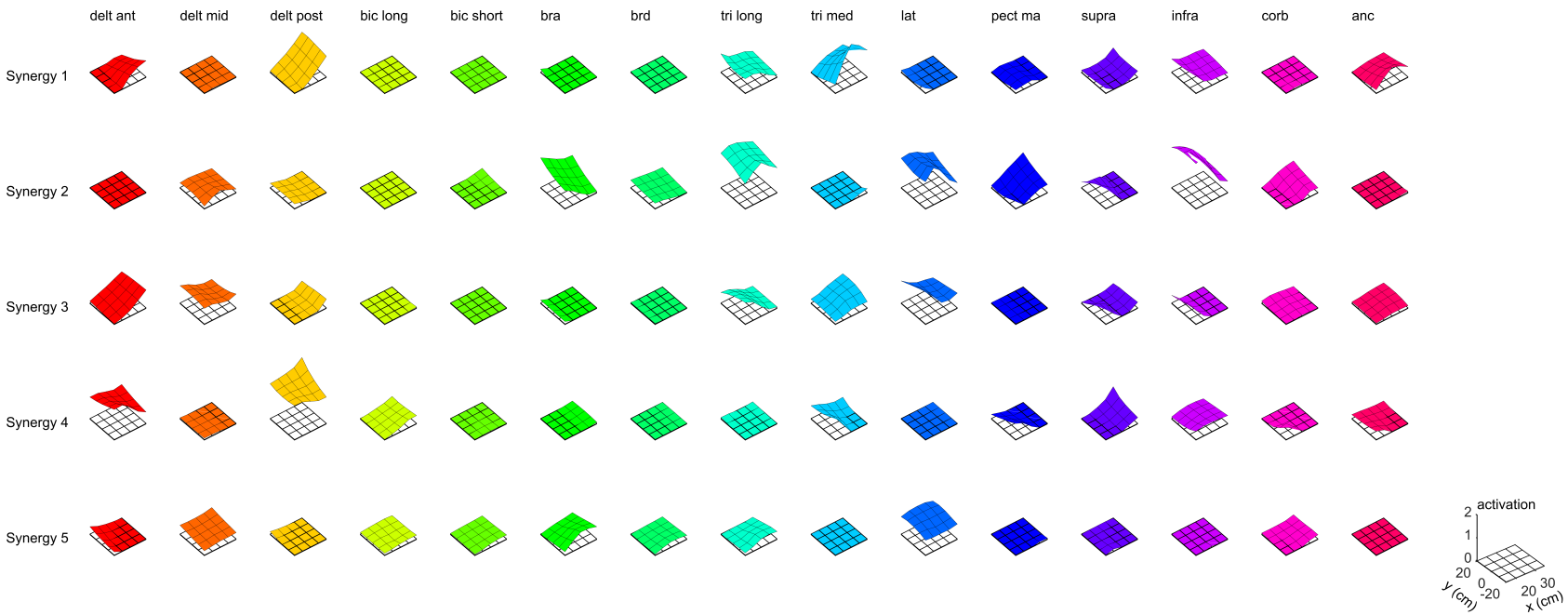

Sup. Fig. 8: Simulation results: detailed muscle activity levels in the synergies